DIFFERENTIAL EQUATION MODELS OF FOREIGN BODY FIBROTIC REACTIONS FOR ASSESSING ROLES OF MACROPHAGE PHENOTYPES AND MESENCHYMAL STEM CELLS

by

LARRISSA OWENS

Presented to the Faculty of the Graduate School of
The University of Texas at Arlington in Partial Fulfillment
of the Requirements
for the Degree of

DOCTOR OF PHILOSOPHY

THE UNIVERSITY OF TEXAS AT ARLINGTON
May 2014

Acknowledgements

This dissertation would not have been possible without the valuable support system I have been blessed with. Jesus Christ whose life encouraged me to serve others, whose death and resurrection gave me the opportunity to embrace a life of purpose, and whose teachings challenged me to be a good steward of the talents he has entrusted to me. My advisor Dr. Jianzhong Su, whose patient guidance and helpful direction drove this research effort. I am grateful for his sensitivity to my goals beyond research, and how that has allowed me to pursue higher education without compromising other callings in my life. My collaborators Akif Ibragimov and Jichen Yang, who have provided valuable assistance with Comsol execution and PDE analysis expertise.

My Husband, Cody Owens, who has supported me, helps speak valuable truth into my life, and bought me so much joy. My parents, Steve and Karen Perkins, who have been supportive and encouraging through my entire education, not letting me give up in grade school when I mistakenly wrote my three's backward, and continuing their support when the day came that the backward "3" became a new powerful symbol, "ε". A symbol which I might add, has in turn served to be far more mathematically relevant lately than "3". I am so indebted to: Amy and Ricky Board, Scott Perkins, Barbara Perkins, Donna Peirson, Robert and Treasa Owens, and The Ash Family because without their prayers and encouragement I would never have made it this far. I am grateful for Howard Payne University Professors Dr. Robert Sartain and Dr. Brett Coulter. They gave me examples of how to serve and mentor students in both life and mathematics and I owe a large portion of my mathematical foundation to them.

I would like to thank my dissertation committee Hristo Kojouharov, Benito Chen, Andrzej Korzenioski, and Chaoqun Liu. I am grateful for the NSF GK-12 (grant # DMS−0908177) and GAANN fellowships that allowed me the financial opportunity to focus on school and service.

April 7th, 2014

Abstract

DIFFERENTIAL EQUATION MODELS OF FOREIGN
BODY FIBROTIC REACTIONS FOR ASSESSING
ROLES OF MACROPHAGE PHENOTYPES
AND MESENCHYMAL STEM CELLS

Larrissa Owens, PhD

The University of Texas at Arlington, 2014

Supervising Professor: Jianzhong Su

Implant failure due to fibrotic encapsulation is an ongoing challenge in the bio-medical field. We develop two mathematical models based on partial differential equations in two spatial dimensions, and use them to gain quantitative insights regarding the dynamics of immune cells and proteins following the insertion of a foreign body. We focus heavily on incorporating a distinction between varied phenotypes of macrophage cells and analyzing their effects on healing processes. We extend our research to a new model that incorporates mesenchymal stem cells that influence the chemical reactions of immune regulators. Stability analysis is conducted on a family of equilibria that correspond to "healed states." Additionally, isolated analysis of key components is presented to allow a more comprehensive understanding of the roles that stem cell presence plays on macrophage population trends. For the purposes of temporal dynamic testing, as well as investigations into the model for which mathematical analysis was cumbersome, computational tools such as MatLab and Comsol were implemented. Model simulations are compared against experimental data as validation to each mathematical model's efficacy.

Table of Contents

List of Figures

List of Tables

Chapter 1

Introduction

The primary objective of this research is to develop and test mathematical models that will enable us to glean a greater degree of understanding into the inner working of fibrotic response to foreign bodies. Studying cellular dynamics at an implant site post-surgery is of great interest because biomedical implants have become an integral part of corrective surgeries. One example, arterial stents, is pictured in Figure 1-1.

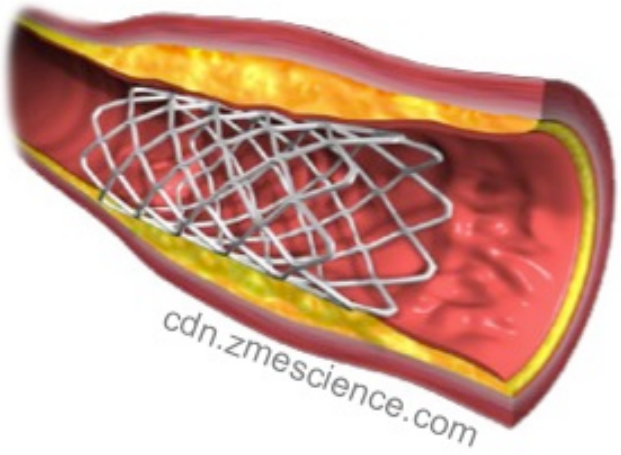

Figure 1-1 Arterial Stent

The human body has a natural immune system that defends the integrity of the body. Commonly, these implants can be prone to persistent inflammation and fibrotic encapsulation leading ultimately to implant failure as a result of the so-called foreign body reactions. Through mathematical modeling we gain greater insight into cellular interactions and their effects on healing processes, and acquire quantitative assessment of the outcomes of foreign body reactions. As predictive models continue to advance, treatment plans can be devised in hopes of lessening the severity of these reactions and decreasing the frequency of implant failure.

1.1 Advantage of Mathematical Modeling

As more and more medical implants are introduced to treat a growing number of patients with varied ailments, the reactions these devices cause have become a common concern for the medical community. While a large amount of experimental data has been accumulated, and great progress made in device improvement and patient care, there is still no comprehensive understanding of the foreign body reaction process. Mathematical modeling can help as the medical community seeks to improve the clinical management of implant fibrotic response by identifying which elements should be manipulated to assist the healing process. Mathematical models provide these theoretical predictions without the need for real-time experiments and help to alleviate the challenges of experimental cost as well as the technical difficulty involved in distinguishing between cell types present in a tissue sample.

1.1.1 The Structure of This Dissertation is as Follows

Chapter 1, we set the stage by providing the biological setting as well as prior mathematical modeling that provide frameworks for our modeling. We provide a preliminary glimpse into foreign body fibrotic reaction modeling and highlight the crucial role that Macrophage populations play in modeling sub-dermal healing processes.

Chapter 2, we introduce our mathematical model that is based on biochemical mechanisms. We test the model against experimental data and record its potential for providing new quantitative insights about foreign body reactions. We conduct a stability analysis of the model to determine quantitative insights about the healing process, with specific attention given to the effect of macrophage phenotypes.

Chapter 3, we add the influence of Stem Cells to our modeling to observe how the presence of Adult bone marrow derived stem cells affect the healing process. We look at the stability of the healed equilibrium state as well as their transient behavior of key inflammatory

mediators to gain insights into the complex cellular reactions involved in implant healing. In Appendix A, an additional model, which includes fibrocyte cell as an additional variable, is also presented and the temporal dynamics are simulated at varied levels of stem cell presence.

Chapter 4 summarizes the results presented in these preluding chapters and provides directions for improving our modeling techniques.

1.2 Biological Background

The process of fibrotic reactions to implants involves several cells and proteins and reacting in a cascade of sequential, parallel and overlapping chemical processes [1].

1.2.1 Foreign Body Reactions at a Glance

Foreign body reactions are often started with the accumulation of coagulation products and the release of various inflammatory products around the biomaterial [1],[2],[3]. The gradient of inflammatory signals leads to the recruitment of macrophages, a type of white blood cell, followed by fibroblasts, a prominent cell type in connective tissue, to surround medical implants [4],[5],[6]. One of the most potent pro-fibrotic products is transforming growth factor-β [7] that can be secreted by activated macrophages [8] or released from damaged or squished cells during the implant insertion [9]. In addition to these initiators, in more recent studies the stimulation of inflammatory mediators is often accredited to activated, resident Mast Cells at the implant site [10].

Once recruited to the implant site by, fibroblasts undergo proliferation and then produce procollagen. Precollege can be converted into collagens by enzymes. Collagen comprises a large percentage of the elements in the extracellular matrix (ECM) that provides scaffolding for new blood vessel stemming (angiogenesis), and in ideal settings fills in around the implant without excessive scar tissue (fibrosis) or inflammation.

The engineering of the surface material and texture of implants has proven to affect the healing process. Furthermore, the coating of an implant with varied chemical, cellular and polymer mixtures has also been a key topic for investigation. The use of certain classes of stem cells and stem cell recruiters to coat implants has shown to promote beneficial macrophage activity and recruitment along with new vessel growth thereby increasing the overall influx of needed cell types [11][12].

1.2.2 Phenotypes of Macrophages

It is well established that macrophages play a pivotal role in wound healing models. Macrophages (MΦ) exhibit remarkable plasticity and can adopt different phenotypes in response to environmental cues [13],[14],[15].

There are at least three known phenotypes of MΦ. Classically activated MΦ, designate as the effector MΦ, are produced during cell-mediated immune response. Interferon-γ and tumor-necrosis factor-α are two of the main signals that promote this phenotype of MΦ. Classical Macrophages have enhanced microbicidal or tumoricidal capacity and secrete high levels of pro-inflammatory cytokines and mediators. Assisted in part by the production of transforming growth factor type β (TGFβ), classical MΦ can help inhibit inflammation through the clearance of apoptotic cells [16], [17].

Wound-healing MΦ (or Inflammatory MΦ) can develop in response to signals through interleukin-4. Arginase activity is stimulated in this phenotype of MΦ, allowing them to contribute to collagen precursors and thereby aid in the production of extracellular matrix [18].

Regulatory MΦ, the final classification of macrophage cells, often arise during the later stages of adaptive immune responses. Their primary role is to dampen the immune response and limit inflammation through the production of interleukin-10 [19].

All three of these phenotypes have been observed experimentally within the dermal wound healing context, and the phagocytes biomaterial interactions are known to be similar here for foreign body reactions.

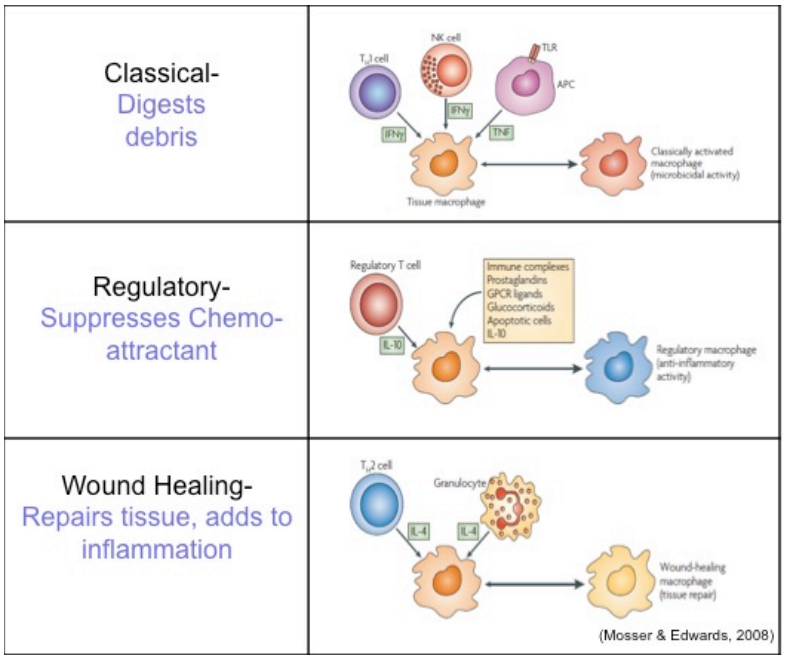

Figure 1-2 Macrophage Phenotypes:
Mosser and Edwards [13] reported on the ability of Macrophage cells to take on different profiles and fulfill varied roles in the wound healing process

1.2.3 Immune Response Initiators

There exist several avenues by which immune response is initiated. The introduction of bacteria and pathogens during surgical process can serve as an initiator for the immune response. Red blood cells or tissue cells that underwent damaged during the implantation also recruit/activate phagocytes (i.e. Macrophages) to the implant site [20].

1.2.3.1 Mast Cells

Furthermore, the initial stage for recruitment of immune cells to the implant site is often attributed to the activation of resident mast cells [21]. Activated mast cells release both histamine

but also interleukin 1-beta (IL1-β) which fall under the category of inflammatory cytokines and signal the up-regulation of macrophage with an inflammatory profile [10].

Once initiation of the immune response has occurred chemoattractants serve to prompt the various cells involved in healing processes to migrate to, or proliferate, at the implant site.

1.2.4 Chemoactractants

Cytokines are crucial for signaling the recruitment of cells that are needed for removing damaged cells, for promoting angiogenic blood vessel stemming, and also for shutting down the immune system to avoid unhealthy inflammation. Recruited cells such as macrophages and fibroblasts continue to release more chemotactic agents to reinforce the gradient fields and to attract more migrating cells.

To help separate these cytokines we classify them into two groups, pro-inflammatory cytokines, and regulatory cytokines (sometimes merely referred to as anti-inflammatory) [1]. These classifications not only help to specify their roles but also establish an association to the macrophage phenotypes that promote them.

Pro-inflammatory cytokines, which includes histamine are released both by inflammatory macrophages as well as during degranulation of activated mast cells, but are inhibited by Regulatory MΦ cells.

Regulatory cytokines consist mainly of interleukin-4 and various growth factors, including Tissue Growth Factors type β (TGFβ), which serve to drive cell proliferation, blood vessel growth and recruitment of macrophages of the regulatory phenotype. These cytokines are released by regulatory MΦ and inhibited by inflammatory macrophages.

We refer to [1] for an extensive list of these two cytokine classifications.

1.2.5 Fibroblasts

Implant-recruited fibroblasts, a cell type in connective tissue, synthesize chains of amino acids called procollagen, a process that is activated by growth factors, including in particular TGFβ to become collagen [22][7].

1.2.6 Extracellular Matrix (ECM)

Enzymes convert procollagen into collagen, the dominant ingredient of the extracellular matrix (ECM) [23].

Similar to collagen formation in dermal wound healing, collagenase is synthesized and secreted by fibroblasts as a zymogen, which is then activated by enzymes to become collagenase. Damaged collagen can also be dissolved by collagenase [24] therefore, collagen degradation and collagen formation are occurring concurrently in a competitive manner.

1.2.7 Angiogenesis

The collagen cells provide a scaffold by which blood vessels can extend into the wound site. This process of new blood vessel growth is called angiogenesis. Both blood and oxygen levels increased by angiogenesis have been known to affect the healing processes [25].

Macrophage cells and Mesenchymal Stem Cells are known to contribute to angiogenesis [26],[12].

Figure 1-3 provides a visual display of the cell populations as they fill in around the surface of a biomedical implant as well as the angiogenesis blood vessel growth as it buds from a nearby blood vessel.

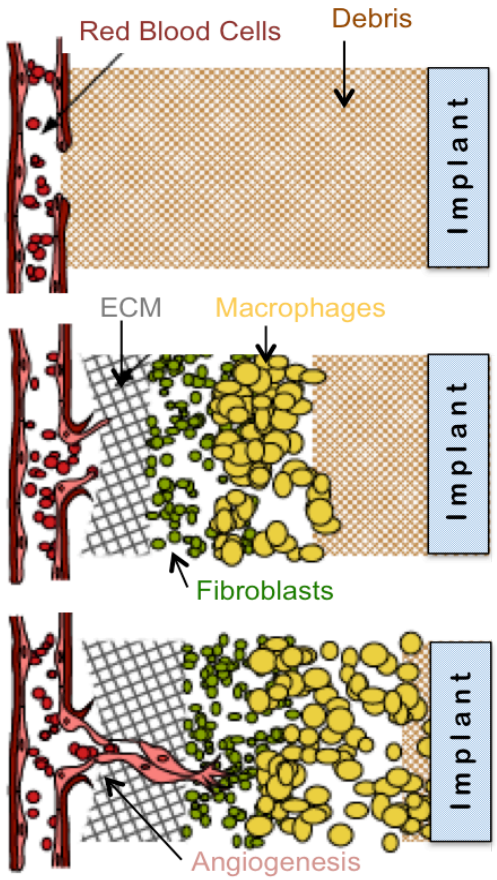

Figure 1-3 Fibrotic Reaction Summary Graphic:
Graphic showing wave fronts that are typically occurring in foreign body fibrotic responses. The debris begins a chemical recruitment of macrophage cells followed by fibroblasts, precursors of collagen cells, which comprise the ECM. These scaffolds provide an opportunity for blood vessels to bud into the newly formed tissue, a process referred to as angiogenesis. This Figure is adapted from a schematic diagram for wound healing [27].

The study of angiogenesis has become very prevalent in modeling tumor growth as new blood vessels provide a nutrition source which tumors count on to grow and spread.

1.2.8 Stem Cells and Stem Cell Recruiters

Changes to the surface texture, the hydrophilic properties, as well as coating the implant with various cells and proteins have shown to impact the anchoring capability of the implant as

well as the scaring and inflammation [28]. A growing interest in experimentation has been in increasing the availability of stem cells at the wound site [29].

Embryonic Stem Cells (ESC) have been of interest to the wound healing community due to their potential to differentiate into the many cells needed to mediate healing processes. However, the ability to control which cell types these ESC's differentiation into is still far from understood [11]. As a result many have turned their attention instead to Adult Stem Cells (ASC), these cells already favor a particular cell linage and are therefore easier to control toward a particular cell outcome.

1.2.8.1 MSCs

Among the ASC class and present in bone marrow, Mesenchymal Stem Cells (MSCs) have the ability to differentiate into cell lineages necessary for wound healing, for this reason we focus on MSCs in our modeling.

1.2.8.2 SDF-1α

Furthermore, to avoid potential rejection of foreign stem cells some studies have extracted MSCs from the bone marrow of the patient prior to surgery [30] and others recruit host stem cells to the wound site through the use of stem cell cytokines such as Stromal Derived Factor-1 alpha (SDF-1α) [28].

Stem cell presence at the implant site has recent been shown to promote the up-regulation of regulatory macrophages, meanwhile inhibiting inflammatory macrophage population growth [28],[31].

1.2.9 Bioengineering Experimental Data

Collaboration with bioengineering labs supervised by Liping Tang provides experimental data concerning key interactions that govern foreign body fibrotic reactions [6][28][4][21]. Figure

1-4 pictures some of the biomedical implants they research. Catheters and stents are tested first within the sub-dermal setting on the back of mice.

Figure 1-4 Samples of Biomedical Implants

The interactions and cellular behaviors they observe help shape the framework of our mathematical models. Furthermore, the stained cell counts that are collected in the lab are then used to help us determine the parameters of our model and test the model's accuracy. For more details on the biological experiments refer to section 2.2.1

1.3 Prior Mathematical Modeling

While experiments are still the main stay in the studying of foreign body reaction related process, significant progress has also been made in detail predictive modeling based on biochemical and biophysics principles. Mathematical modeling of biological process has been a long building exploration. In fact, several of the modeling relationships we use in modeling cellular interactions can be traced back to the techniques of Malthus and Verhulst in the 18th and 19th centuries, where differential equations were developed to model exponential growth and decay of populations as well as the logistic growth that accounted for populations impacted by saturation levels. In the early 20th century a great contribution by Lotka and Volterra brought about a way to account for predator and prey relationships. Using population dynamics at a cellular level has yielded great insights into the immune response. These modeling tools allow us

to explore cellular interactions and healing processes of post-surgery implants. Prior to our sub-dermal applications, dermal wound healing served as a prominent application for wound healing modeling techniques.

1.3.1 Wound Healing

For dermal wound healing, basic reactions were first considered in studies by Dale et al 1996 [32], 1997 [33]; Dallon et al 2001 [34] and many others.

Figure 1-5 provides the schematic used by Dale [32] to outline the reactions between the cells and proteins involved in wound repair processes. The Dale model [32] leads to system of sixteen, coupled ODEs that quantify the activations, conversions, secretions, proliferations, and apoptosis of 2 collagen cell types and their precursors.

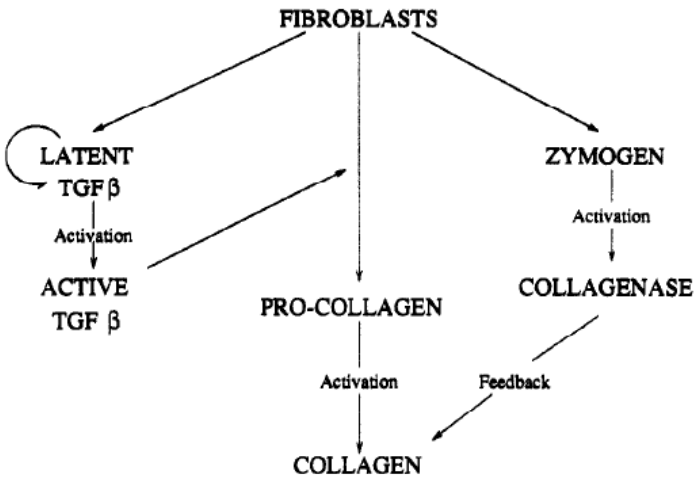

Figure 1-5 Dale Model Schematic:
Dale et al [32] created a system of 16 coupled ODEs that accounted for the reactions outlined here. Not explicitly pictures are the 3 enzymes that are driving the activation. Also since two collagen cell types are being studied, all cells and proteins in the schematic take on two separate variables (with fibroblasts being the one exception as both collagen populations stem from the same fibroblast cell type).

The Dale model was successful is investigating the effects that two different types of TGFβ have on scar formation and found that the simulation results of their model compared favorably with experimental data. In section 1.3.3 below we will return to the Dale et al model

and discuss the expansion they made to their model to include cell diffusion and wave-like migration [33].

In 2006 Waugh and Sherratt [35] developed a reaction-based model that they referred to as "deliberately simple." It isolated macrophage dynamics at a wound site. With only three variables, their model consisted of two categories of macrophage cells, inflammatory and repair, as well as the concentration TGFβ. The model brought insights of the impact that macrophage phenotypes have on the delayed healing that many diabetic patients have experienced.

1.3.2 Fick's Law

Fick's Law allows us to expand mathematical modeling beyond isolated reaction terms occurring between species/cells and allows us to account for cell movement and migration. Diffusion, which serves to imitate the random motion of particles, and Chemotaxis, which accounts for an attractant and models motion being directed up a concentration gradient, can both be describe using a flux [36].

Fick's law defines a simple model of the flux, J, of a chemical species, u, by

$$J = -D\nabla u$$

where D is the diffusion coefficient, ∇ is the Laplacian, and ∇u represents the gradient of the species population. This characteristic, where movement is driven opposite of the gradient, when applied to the conservation law for population affected by transport,

$$\frac{du}{dt} = -\nabla \cdot J + (\text{local production of } u)$$

yields a reaction-diffusion equation for modeling cell movement.

1.3.3 Reaction-Diffusion Models

Reaction-Diffusion equations account for local source terms, f, caused by chemical reactions as well as this flux, J, and are of the form:

$$\frac{du}{dt} = D\nabla^2 u + f$$

The reaction terms, f, are often visualized in schematic form as was done in the Dale model (refer to section 1.3.1 above).

In 1997 the Dale model was expanded to include chemical diffusion among the chemoattractant and fibroblast terms.

The migration cells, u, are often attracted by a chemoattractant field, c. This mediation by a gradient sensing mechanism can be captured by chemotactic flux terms, $\nabla u \chi \nabla c$, with the strength of the chemotaxis accounted for in the chemotaxis parameter, χ. Fibroblast and Macrophage migration are both modeled in this way.

In 2008, Schugart et al. [25] published a reaction-diffusion model for wound healing which combined all the chemoattractants into one variable and modeled the interactions between collagen, fibroblasts, and macrophages. In addition to these cell types, Schugart included angiogenesis equations to the healing process and examined the positive effects of increased oxygen level in accelerating the healing and closure of open wound, suggesting new insights for the healing.

Through interactions between immune mediators, phagocytes in the blood and tissue, the acute inflammatory response was modeled and analyzed by reduced compartmental models in Reynolds et al 2006 [20] and Day et al 2006 [37]. Atherogenesis in blood vessels was modeled by continuum equations in Ibragimov et al [38].

The initiator for immune response is often modeled using a debris term that prompts phagocytosis [20], [37], [38]. We make this assumption in our modeling as well, assuming that the digestion of dead cells (or tissues) initiates the entire healing process.

1.3.4 Modeling Sub-dermal Healing Processes

The cells involved in healing processes following the surgical insertion of an implant follow closely with the pathways involved in dermal wound healing. These processes may differ, however, in specific activation and inhibition loops. We draw modeling techniques from work conducted for surface wounds and adapt the work to correlate with the altered environment of the sub-dermal setting.

In particular, Macrophage (MΦ) cells play a more prominent role in the activations and inflammations within the setting of post-implant healing. Also, since Foreign Body reactions are multiple time-scale processes, the initiation process happens in a much short period of time when compared with other processes. This allows us to simplify modeling by assuming active/inactive protein, growth factors have already reached balance, and thus, we get a reduced system of fewer equations for our foreign body reaction model.

We share a portion of our previously published results from [39] to provide a preliminary glimpse as to how incorporating the roles of macrophages can assist in adjusting wound healing models so that they can be applied to sub-dermal contexts. Figure 1-6 helps demonstrate this principle. The 1997 Dale model [33] simulates collagen population as having asymptotical behavior as going to infinity linearly. The unbounded results of the Dale model, while successful for modeling dermal wounds, are inconsistent with the sub-dermal healing context due to the finite space present between an implant and the surrounding healthy tissue. This inconsistency warrants a need for incorporating Macrophage cell populations into the foreign body reactions model. This incorporation is accomplished in a modified Dale Model and is presenting in full in our 2011 work, [39].

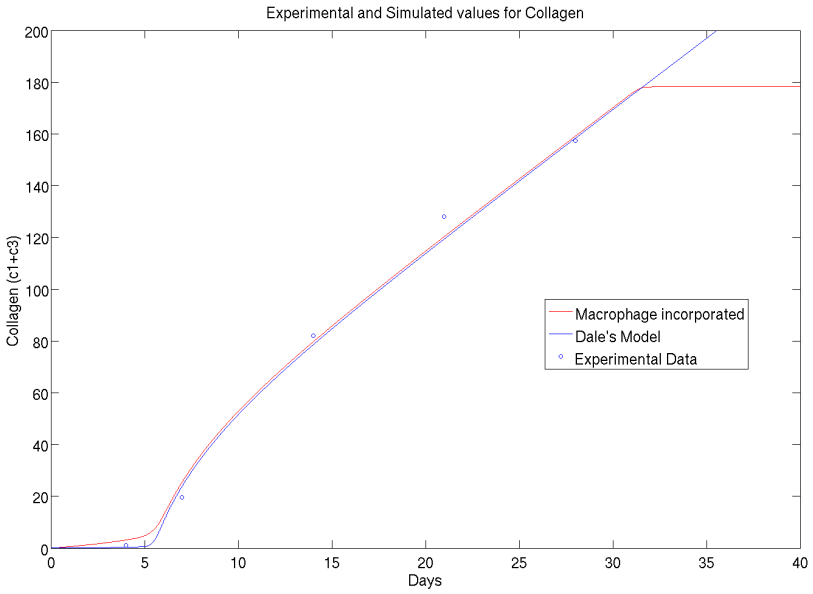

Figure 1-6 Modified Dale Model Accuracy:
The comparison of collagen level in experimental data (the average value of samples during a 28-day period, unit: ug/cm2) with simulated data from both Dale models. The classical Dale model[33] with parameters fitting for Foreign Body Reactions (blue) simulates a collagen population that increase linearly as time increases, producing an asymptotically unbounded growth. Our improved foreign body reaction model [39]incorporates MΦ cell and the modified model (red) is shown to have a realistic behavior of the collagen cell population.

Specifically, the Modified Dale Model [39] differs from early collagen models primarily because it incorporates the following features: (a) Macrophage produce procollagens specific enzymes at a near-saturated level, (b) Macrophage regulate collagen growth through productions of zymogens, and (c) Macrophage phagocytic behavior in clearing of apoptotic cells, which can lead to an inhibition of inflammation. In keeping with the 1997 publication of the Dale model [33], which extended to include chemical diffusion among the chemoattractant and fibroblast terms, we also account for diffusion of the macrophage population in the Modified Dale model. Figure 1-6 shows these new features with collagen cell concentrations at an implant simulated over a 40-day healing period.

1.3.5 Incorporating Stem Cells in Modeling

In 2009 Lemon et al created an ODE to model the temporal dynamics of angiogenic processes at an implant site [29]. The model accounted for a stem cell coating on the implant scaffold. The rate of change of the stem cell count consisted of a proliferation term, affected by the amount of unoccupied space at the implant site as well as oxygen concentrations, and a decay term (also affected by oxygen concentrations). Stem cell count affected the chemoattractants involved in angiogenesis. The chemoattractant uptake and decay was assumed to reach quasi-steady because its biochemical reaction is sufficiently fast in relation to the time scales of the other biochemical reactions considered in the modeling (i.e. macrophages, fibroblasts, capillaries, pericytes, and ECM).

Jain et al [40] created a model consisting of coupled ODE and PDEs that also explored the impact of stem cell coatings on sub-dermal healing processes. Their simplified Stem Cell modeling consisted purely of an exponential decay term of stem cells. Furthermore, stem cells were modeled to affect angiogenesis solely by up-regulating the proliferation of adipocytes. They separated the stem cell affects from other variables of the foreign body response. Included in these other variables is an inflammatory cell population that grouped macrophage and fibroblast populations together in one term. This term then promoted a variable representing collagen and giant cell populations. The model [40] was broken into two sub-models, one focused on inflammatory cells affecting vascularization, and the other focusing on the stem cell impact. They used the model to investigate the ideal thickness of stem cell coating (so that stem cells would not die off before the wave of adipocytes reached the implant) but also recognized the need for their sub-models to be combined before an accurate representation could be reached. Biologically it is understood that stem cell affects are not isolated from the inflammatory affects and while combining the Jain sub-models leads to a system of 7 differential equations, their paper concluded by stating this need as their continued work [40].

Chapter 2

Two-Dimensional Model

In this chapter we begin by presenting a 2-Dimensional computational model to systematically study the complex dynamics of foreign body reaction processes. The model is based on kinetics of foreign body reactions with both macrophages and fibroblasts playing major roles. We test this model numerically in the same physical setting as in an implantation experiment in mice. The computer-simulated results are compared with the experimental dataset. Both kinetics trends of cell population distributions in 2-D spaces and experiments/modeling discrepancies are obtained for this comparative study. The modeling results (portions of which are published in [1]) indicate the consistent trend of the cell populations as shown in experimental data and in modeling studies, affirming the value of mathematical modeling in serving as a predictive tool for developing plausible experimental hypotheses. We draw further conclusions about how varying macrophage phenotype dominance can affect healing processes by investigating the stability of the equilibrium representative of the "inflamed state" (published in [42]).

2.1 Chemical Kinetic Equations with Macrophage Phenotypes

As mentioned in the introduction, macrophages have been categorized into populations based on three different homeostatic activities – host defense, wound healing and regulation, as have been observed experimentally. The varied responses from three kinds of macrophage cells – classical, inflammatory and regulatory macrophage cells – may affect not only the fibroblast proliferation but also the whole foreign body reaction procedure. We incorporated this important feature into our model which is partially from the mass-action kinetics framework developed by Schugart et al. [25] but used a simplified model in cell and collagen (or extracellular matrix, ECM) growth to avoid over-complication of our study.

We added new kinetics of macrophages reactions into the framework so that we can generally capture the kinetic characteristics of fibroblasts and macrophages and gain more insights on how different macrophage populations regulate the foreign body reaction processes. We aim to find the variations between tissue responses at different population mix of classical, inflammatory and regulatory macrophages during the foreign body fibrotic reaction process.

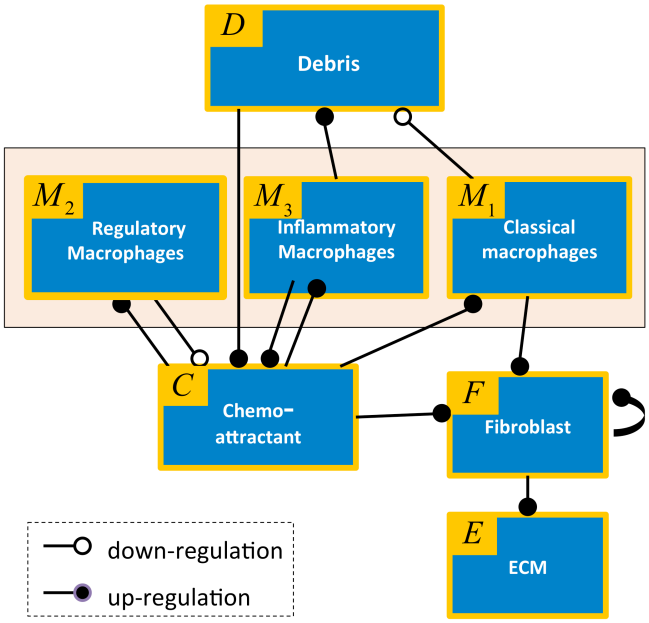

Figure 2-1 Reaction Schematic:
This schematic summarizes the biological feedback loops between the cells and cytokines included in our modeling.

Before we introduce the mathematical equations, we lay out basic hypotheses of the biological process in foreign body reactions:

- A debris cell population, consisting of foreign body damaged cells, blood clots and other injury-released cells, triggers foreign body reactions.
- A generic growth factor such as vascular endothelial growth factor (VEGF) regulates fibroblasts and macrophages through chemotaxis. The chemoattractant undergoes

random motion and its concentration is assumed to grow in proportion to secreting inflammatory macrophages but is suppressed by regulatory macrophages.

- Fibroblast represents a main cell type in secreting collagen/ECM during healing. Its proliferation and collagen synthesis are up-regulated by the chemoattractant gradient field as well as being directly up-regulated by classical macrophages through TGFβ.
- Macrophages act in different roles during foreign body reactions according to their phenotypes as classical macrophage, inflammatory macrophage or regulatory macrophage. The proliferation of macrophages is through diffusion and migration up-regulated by the chemotactic gradient field, and cell apoptosis is also assumed.
- Fibroblasts secrete procollagen which is then activated by TGFβ into collagen (or ECM). ECM diffusion, fibroblast movement, chemotactic migration, and ECM saturation are factored into a mass-action law.

We model the fibrotic reactions as follows:

$$\frac{\partial D}{\partial t} = D_0\nabla^2 D - f_0 M_1 D + \tilde{f}_0 M_3, \tag{4.1}$$

$$\frac{\partial C}{\partial t} = D_1\nabla^2 C + f_1 d + f_2 M_3 - f_3 M_2 C - f_4 C, \tag{4.2}$$

$$\frac{\partial F}{\partial t} = D_3\nabla^2 F - \nabla(\alpha F\nabla C) + a_1 M_1 + a_2 F(1 - F/F_0) - a_3 F, \tag{4.3}$$

$$\frac{\partial M_i}{\partial t} = D_2\nabla^2 M_i - \nabla\left(\alpha H\left(M_0 - \sum_{i=1}^{i=3} M_i\right)M_i\nabla C\right) - a_0 M_i,\ i = 1,2,3\ , \tag{4.4}$$

$$\frac{\partial E}{\partial t} = D_4\nabla^2 E + \nabla\frac{a_4 D_5 EF}{F_0}\nabla F - \frac{a_4\beta EF}{F_0}H(F_0 - F)\nabla C + a_5 F(1 - \frac{E}{E_0}). \tag{4.5}$$

Here, the debris cell population $D = D(x, y, t)$ represents dead tissue or excessive cells following an implantation. We assume debris cells are digested by M_1-classical macrophages but the accumulation of M_3-inflammatory macrophages contributes to the debris during the healing process. The chemoattractant $C = C(x, y, t)$ consists mainly of various forms of TGFβ released during the healing. The chemoattractant field is enhanced by the presence of debris cells and

inflammatory macrophages, but is inhibited by regulatory macrophages. We assume that cell migration is through diffusion and chemotactic migration. Fibroblast proliferation and collagen synthesis are up-regulated by the chemoattractant gradient field. Thus fibroblast population, $F = F(x, y, t)$, can be approximated by a chemically enhanced logistic growth $F(1 - F/F_0)$ with a carrying capacity F_0, along with its diffusion in space modeled by $D_3\nabla^2 F(x, y, t)$, chemotactic migration by $\nabla(\alpha F \nabla C)$ and its natural decay according to time. The macrophage density, $M(x, y, t)$, is the summation of M_1 - classical macrophages, M_2 - regulatory macrophages, and M_3 - inflammatory macrophages. We assume that they each take on $\lambda_1, \lambda_2, \lambda_3$ proportions of macrophages, respectively. Each macrophage phenotype may behave differently at different stages of foreign body fibrotic reactions. Our model simplifies the situation in that (a) the proportion of $\lambda_1, \lambda_2, \lambda_3$ for different phenotypes of macrophages is taken to be fixed; and (b) the three macrophage populations are set to share one common biochemical reaction as their basic biochemical properties are similar. The migration of macrophages at the field is through diffusion and convection along the chemotactic gradient field. The proliferation of macrophages is also up-regulated by the chemoattractant, but their production does reach a limiting value once macrophage population reaches saturation. Macrophage cell apoptosis is also assumed. Finally, fibroblasts secrete procollagens and the product is activated by chemoattractant TGFβs into the collagens or ECM at the quantity $E = E(x, y, t)$. We also incorporate the effects of ECM diffusion, fibroblast movement, chemotactic migration and ECM saturation in mass-action law. Here H is the Heaviside function, and M_0 is macrophage saturation level.

2.2 Testing Model Dynamics Against Experiment

2.2.1 Experimental Data

Experiments on wound healing were performed using a rat subcutaneous implantation model [43]. The animal experimental protocol was approved by the University of Texas at

Arlington Animal Care and Use Committee. Briefly, cylindrical polyethylene catheters (1.0 cm. in radius and 5 cm. in length) were sterilized with multiple washes of 70% ethanol. Then the tubes were implanted in the subcutaneous space on the back of Sprague Dawley rats (~200 grams body weight). The incision was then closed with stainless wound clips.

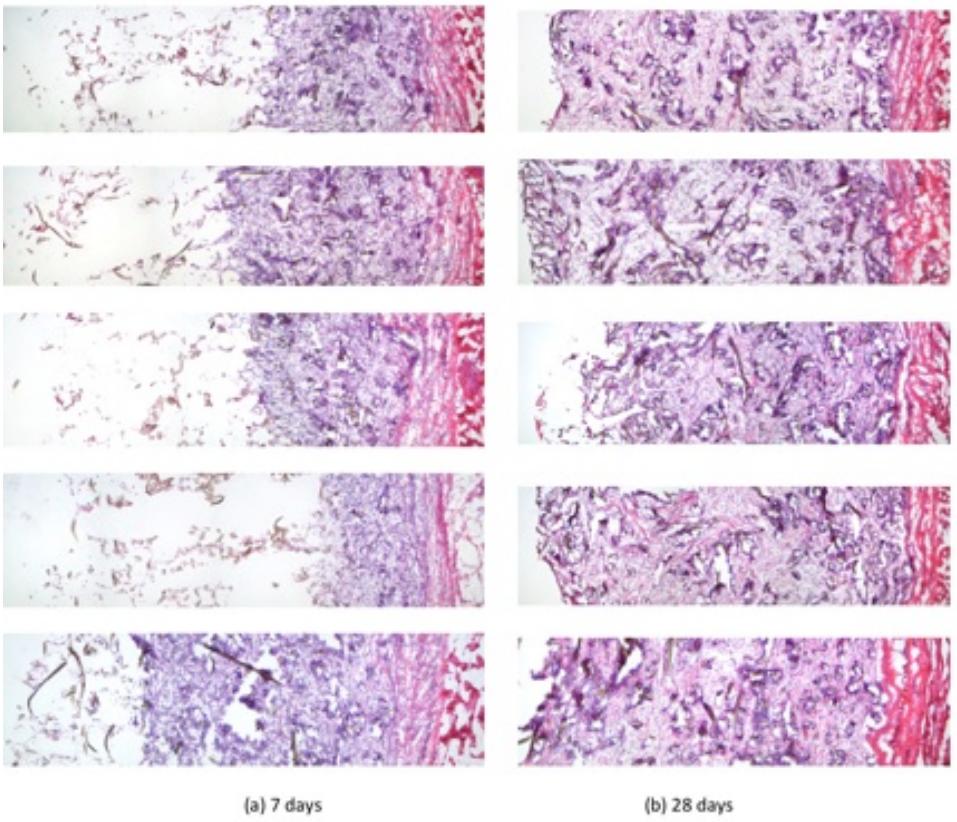

Figure 2-2 Experimental Slices

The experimental slices with fluorescent dye. Here the left side of the image represents a location directly adjacent to the implant. (a) Left column shows slices obtained from 5 mice have been implanted disks for 7 days. (b) Right column shows slices obtained from 5 mice have been implanted disks for 28 days.

After implantation at different periods of time (7 and 28 days), the animals were sacrificed. The implants and surrounding tissue were isolated for histological analyses [6],[44]. For quantifying the numbers of fibroblasts and macrophages, tissue sections were stained with α-smooth muscle action and MOMA-1, respectively. The experiment design sketch is presented in

Figure 2-3, the experimental tissue slices are pictured in Figure 2-2, and the cell counts from these expirements are recorded in Table 2-1.

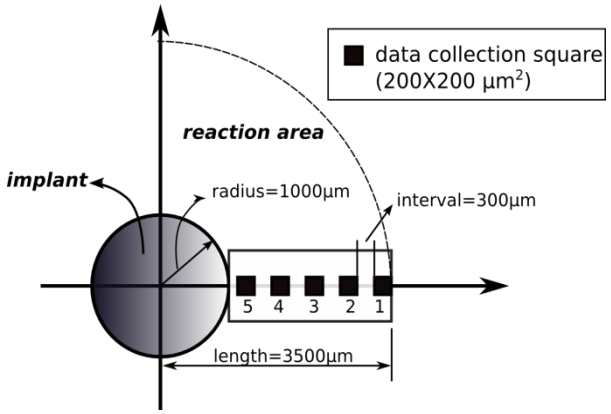

Figure 2-3 Data Collection Proximity to Implant

Table 2-1 Experimental Data of Fibroblasts and Macrophages

7 days										
Area / mouse	1		2		3		4		5	
	fibroblast	Macrophage	fibroblast	Macrophage	fibroblast	Macrophage	fibroblast	Macrophage	fibroblast	Macrophage
#1	50	138	39	124	29	138	17	24	0	0
#2	30	129	29	100	41	51	32	53	0	0
#3	39	80	46	50	29	20	0	0	0	0
#4	27	80	17	59	0	0	0	0	0	0
#5	25	84	18	82	38	60	39	45	0	0
Ave.	34.2	102.2	29.8	83	27.4	53.8	17.6	24.4	0	0
28 days										
Area / mouse	1		2		3		4		5	
	fibroblast	Macrophage	fibroblast	Macrophage	fibroblast	Macrophage	fibroblast	Macrophage	fibroblast	Macrophage
#1	28	78	47	38	51	30	42	21	69	18
#2	44	86	65	47	57	10	59	43	54	37
#3	53	80	100	40	50	34	62	18	17	12
#4	32	86	80	56	73	22	49	31	66	20
#5	40	54	74	43	63	30	73	44	51	30
Ave.	39.4	76.8	73.2	44.8	58.8	25.2	57	31.4	51.4	23.4

2.2.2 Boundary and Initial Conditions

We simulated the kinetics based on the model under the assumptions that all the functions are defined in the reaction domain which is an annulus $G = \{(r,\theta), L_{in} \le r \le L_{out},\ 0 \le \theta < 2\pi\}$, where the inside disk $\{(r,\theta), 0 \le r \le L_{in},\ 0 \le \theta < 2\pi\}$ is the location of the implant, the

outside ring $\{(r,\theta), L_{out} \leq r < \infty,\ 0 \leq \theta < 2\pi\}$ is the normal surrounding tissue.The set of points $\{r = L_{in}\}$ represents the inner edge of the wound i.e., the outer edge of the implant. $\{r = L_{out}\}$ represents the outer edge of the wound. Along the outer edge of the wound, it was assumed that the densities of fibroblasts and ECM remain constant at the level of the unwounded state. Along the inner edge of the wound, it was assumed that the density of debris remains in a wounded state caused by the implant. The densities of the macrophages were assumed to decrease at the boundary of the healthy tissue as the healing process progressed and the flux of the chemoattractant on this boundary was negligible.

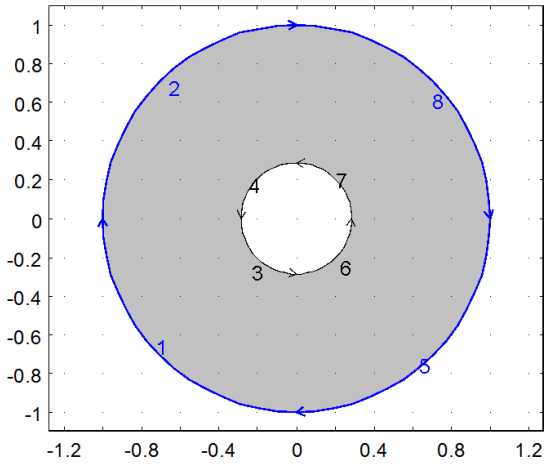

Figure 2-4 Boundary Conditions:
At the outer edge 1, 2, 5, and 8, F = F_0, M = $M_0 e^{-\gamma_2 t}$, E = E_0, $\frac{\partial C}{\partial r} = 0$, where γ_2 is the decay coefficient at the boundary for macrophages; at the inner edge 3, 4, 7, and 6, D = $\overline{D}_0$. The axes present dimensionless values

As shown in Fig.1, at $r = L_{out}$ the boundary conditions are as follows,

$$F = F_0,\ M = M_0 e^{-\gamma_2 t},\ E = E_0,\ \frac{\partial C}{\partial r} = 0.$$

At $r = L_{in}$, the boundary condition includes

$$D = \overline{D}_0.$$

In all other cases, the following no-flux boundary conditions are used,

$$\frac{\partial F}{\partial r} = \frac{\partial D}{\partial r} = \frac{\partial M}{\partial r} = \frac{\partial E}{\partial r} = \frac{\partial C}{\partial r} = 0.$$

The initial values are set at $t = t_0$, and are taken to be a distribution. The formula is

$$\frac{X}{X_0} = \left(\frac{r - L_{in}}{L_{out} - L_{in}}\right)^2 e^{-\left(\frac{L_{out} - r}{\varepsilon(L_{out} - L_{in})}\right)^2},$$

where $X = C, F, M, or\ E$, and ε is selected such that all the densities are initially near zero away from the wound outer edge. For debris, the initial distribution follows the formula

$$\frac{D}{D_0} = \left(\frac{L_{out} - r}{L_{out} - L_{in}}\right)^2 e^{-\left(\frac{r - L_{in}}{\varepsilon(L_{out} - L_{in})}\right)^2}.$$

2.2.3 Simulations and Dynamics of the Model

In our simulation study, we placed a circular-shaped implant at the center of a reaction domain. Healthy tissue was positioned immediately adjacent to the reaction domain where these normal cell/protein/enzyme values were imposed as boundary conditions. Then, we calculated the densities for macrophages and fibroblasts from area 1 to area 5 on day 7 and day 28, respectively. Because we counted the number of macrophages and fibroblasts from our experimental results, which were not the densities that we can only derive from our simulations, we scaled our simulation results by multiplying a factor to fix the simulation result at area 1 on day 7 same to experimental data. Then we multiplied the same scale ratio to the simulation results at other areas on day 7 or day 28. Based on this scale strategy we can observe and compare the trends between simulations and experimental data for the proliferation of macrophages and fibroblasts.

2.2.4 Macrophages Dynamics Simulation vs. Experimental Data

Here, we present the simulation results of macrophages on day 7 and day 28. The graph in Figure 2-6 (A) shows the macrophages' distribution for five mice while Figure 2-6 (B) shows the comparison between the simulation and the average of the experimental data on day 7. Similarly, Figure 2-7 shows the simulation and the average of the experimental results on day 28. The three dimensional pictures of the macrophages densities are presented in Figure 2-5.

Furthermore, because we set a time-varying Dirichlet boundary condition for the macrophages, the whole density level of macrophages decreased from day 7 to day 28. This is consistent with what we observed in our experimental data. The distributions of the macrophages in our simulation results are consistent with those derived from the experimental data.

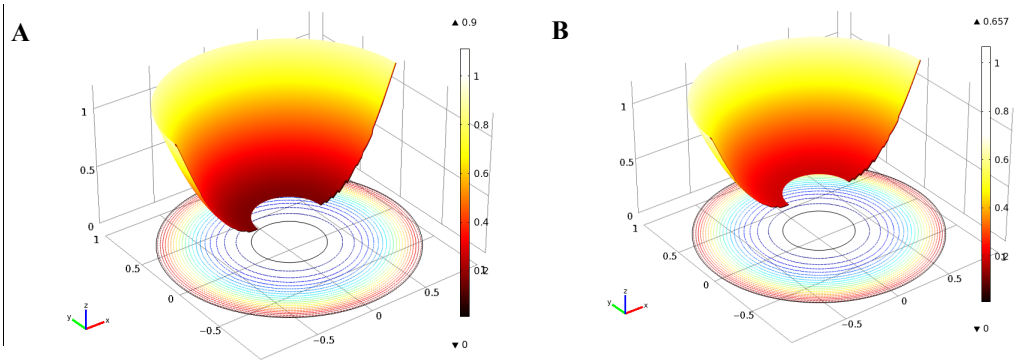

Figure 2-5 3D Simulation- Propagation of Macrophage Cells
(A) t=7, (B) t=28

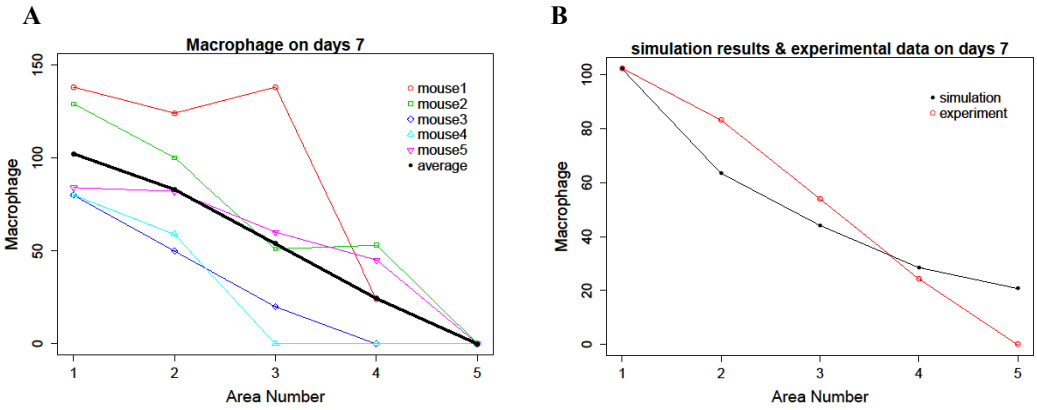

Figure 2-6 Simulated Data for Macrophages at Day 7
(A) 7th day experimental data (all five mice) plotted together with the average curve;
(B) average experimental data versus the simulated result on day 7.

B

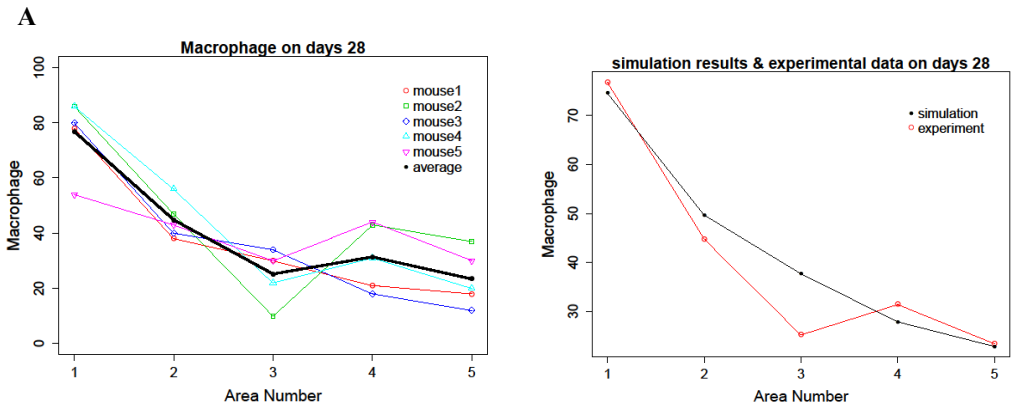

Figure 2-7 Simulated Data for Macrophages at Day 28
(A) 28th day experimental data (all five mice) plotted together with the average curve;
(B) average experimental data versus the simulated result on day 28.

2.2.5 Fibroblast Proliferation Simulation vs. Experimental Data

Next we present the simulated fibroblast growth near an implant. The statistical results comparing the model simulation and the experimental data for fibroblasts on day 7 and day 28 are shown in Figure 2-9 and Figure 2-10, respectively. From Figure 2-9(B) and Figure 2-10(B) we can see that, although the simulation results for fibroblasts do not fully agree with the experimental results, the trends of the simulation curves are similar to those derived from the experimental data. We note that in Figure 2-10(B), the difference between two curves is relatively big. This may be caused by the boundary condition. As mentioned before, we set a constant value for the Dirichlet boundary for fibroblast based on our assumption that the density of fibroblast in healthy tissue is a constant value. This assumption is also applied in Schugart 2008 [25]. This may be the reason that we observe the simulation result at area 1 on day 7 to be very close to the experimental value at area 1 on day 28. But from our experimental data we noted the fibroblasts increased at area 1 from day 7 to day 28. This difference on boundary may cause the magnified discrepancies in other areas during the evolution.

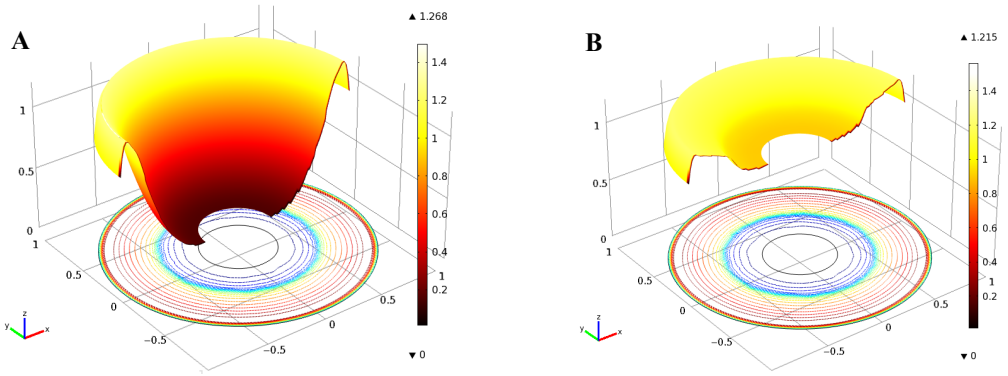

Figure 2-8 3D Simulation- Distribution of Fibroblast Cells
(A) t=7, (B) t=28

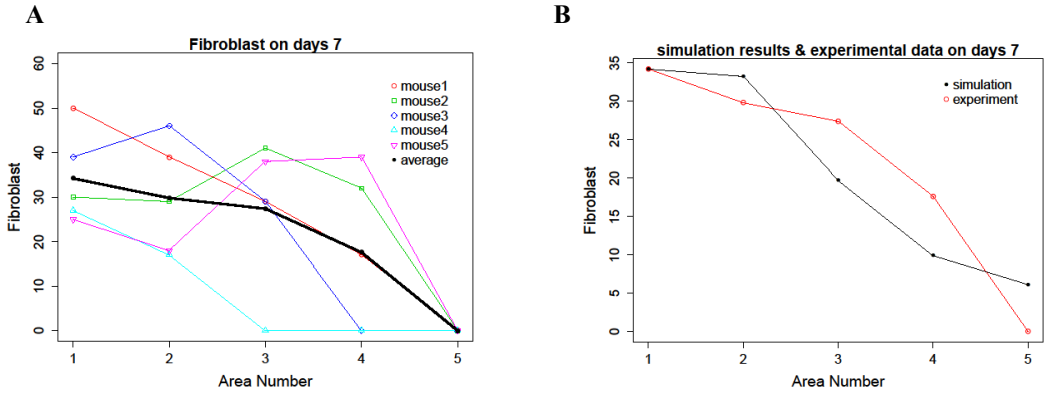

Figure 2-9 Simulated Data for Fibroblast at Day 7
(A) 7th day experimental data (all five mice) plotted together with the average curve; (B) average experimental data versus the simulated result on day 7.

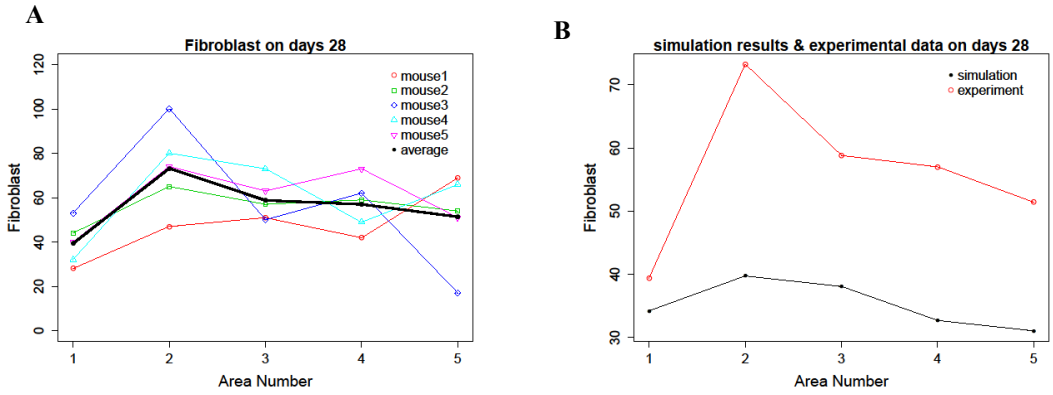

Figure 2-10 Simulated Data for Fibroblast at Day 28
(A) 28th day experimental data (all five mice) plotted together with the average curve;
(B) average experimental data versus the simulated result on day 28.

We have observed that there is a discrepancy between the model and experimental data, and this is more significant for fibroblast population than macrophage. One plausible reason is the ideal boundary condition that we have imposed for the fibroblast. If you recall from Boundary and Initial Conditions, the fibroblast population adjacent to the healthy tissue is assumed to be a constant, whereas the experimental data shows an increased amount of fibroblast along the boundary, partially due to the extra supply from nearby blood vessels' expansion. This discrepancy in boundary conditions explains why the model predicts a lower estimate of fibroblast populations. It is however difficult to account for this blood supply in the system as the mechanism of blood vessels is quite complex.

2.3 Impact of Different Macrophage Phenotypes on Temporal Dynamics

In this section we analyze impact of the different phenotypes of macrophages on the dynamics of the process and trends in proliferation of fibroblasts. Macrophages are capable of secreting growth factors that are important in regulating fibro-proliferation. Alternatively activated macrophages overexpress certain extracellular matrix proteins, such as fibronectin, and are believed to be involved in tissue remodeling during wound healing. Human macrophages activated by biomedical polymers in vitro have been shown to stimulate fibroblast activity. Therefore, biomaterial adherent macrophages can help modulate the formation of fibrous capsules, which develops around a material following implantation.

An important feature we found through modeling study is that the compositions of macrophage phenotypes affect both the timing of fibrotic reactions as well as the macrophages presence.

We tested temporal dynamics of Eq.(4.1)-(4.5) by assuming the chemoattractant is instantaneously available. In doing so, we choose parameters in a typical set of parameter as in [25], furthermore, we incorporate a proliferation term for macrophage and fibroblast populations under the influence of c. and neglected all spatial variations. By taking the initial values to be

$D(0)=1,\ C(0)=F(0)=M(0)=E(0)=0.01$ a few interesting observations (shown in Figure 2-11) were obtained through numerical simulations. It can be seen that debris is cleared out much faster when the classical macrophage is taken to be the dominant phenotype in the reaction. Also we see that an inflammatory macrophage dominated reaction leads a much earlier proliferation of growth and fibrotic actions to occur. Furthermore, reactions in which the dominating phenotype was taken to be either classical macrophages or regulatory macrophages both resulted in similar actions, but inflammatory macrophage dominated reactions did display much higher inflammation. In Figure 2-11 we observe big differences in chemoattractant when the compositions of macrophage phenotypes are switched, especially in inflammatory macrophage dominated case.

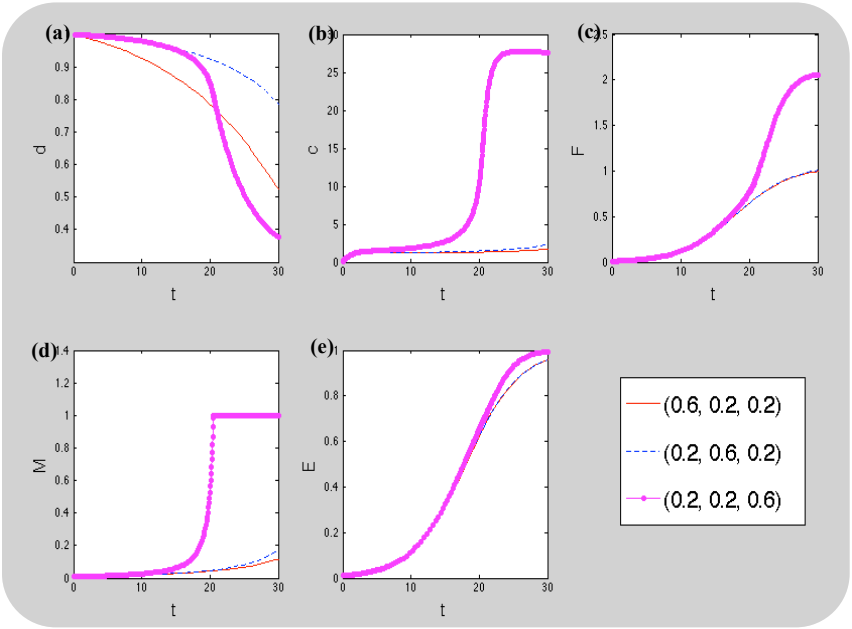

Figure 2-11 Computational Results for Foreign Body Reaction Processes at Different Compositions of Macrophage Phenotypes

λ_1, λ_2, and λ_3 are the proportions of macrophages for M_1- classical macrophages, M_2- regulatory macrophages, and M_3- inflammatory macrophages, respectively. $(\lambda_1, \lambda_2, \lambda_3) = (0.6, 0.2, 0.2)$ is captured in red, blue represents the ratio at $(0.2, 0.6, 0.2)$, and magenta is at the ratio $(0.2, 0.2, 0.6)$. The variables are (a) debris, (b) chemoattractant, (c) fibroblast, (d) macrophage, and (e) ECM.

We now use the parameter set that is specifically chosen to match this experiment. We observe (in Figure 2-12) that with the exception of debris and chemoattractant, the three phenotypes did not cause much difference in reaction alone. In particular, the macrophage total amounts are shown as decreasing in all cases. We predict therefore that the changes in macrophage in our experimental setting of implant inflammatory reactions are mainly due to diffusion and chemotaxis, rather than proliferation. This is a fact that can be further tested in experiments

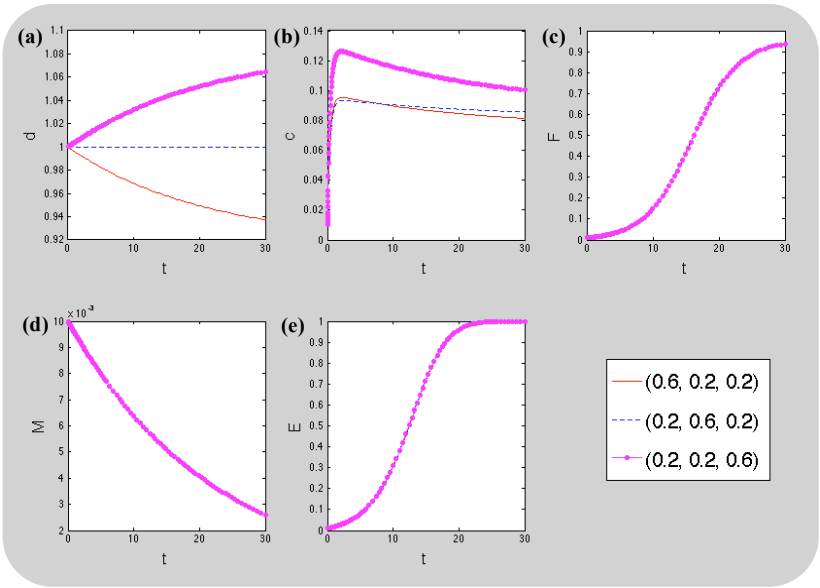

Figure 2-12 Computational Results at Different Compositions of Macrophage Phenotypes Under Parameter Table

λ_1, λ_2, and λ_3 and variables are defined the same as in Figure 2-11.$(\lambda_1, \lambda_2, \lambda_3) = (0.6, 0.2, 0.2)$ is captured in red, blue represents the ratio at $(0.2, 0.6, 0.2)$, and magenta is at the ratio $(0.2, 0.2, 0.6)$. The variables are (a) debris, (b) chemoattractant, (c) fibroblast, (d) macrophage, and (e) ECM.

2.3.1 Parameter Values

Table 2-2 lists the parameters in both dimensional and dimensionless form. Similar to the method introduced in [25], we converted the dimensional parameters to dimensionless units when conducting simulation studies.

In our study, L_{out} is 0.35 centimeters and L_{in} is 0.1 centimeters. For the parameters D_1, f_4, D_2, α, F_0, a_3, α', a_0, D_5, D_3, β, and E_0, the estimated values were derived from literatures and were handled in the same way introduced in [25]. For the parameter D_0, we assume the diffusion rate for debris is lower than the other diffusion rates. Although the precise value was not known, D_0 was chosen to be 1.0E-5 as its dimensionless value.

Table 2-2 Table of Parameters and Boundary Conditions

Parameters	Dimensional Value	Source (CS-Current Study)	Dimensionless value
$\boldsymbol{L_{out}}$	0.35 cm	CS	1
$\boldsymbol{L_{in}}$	0.10 cm	CS	0.286
$\boldsymbol{D_0}$		CS	1E-5
$\boldsymbol{f_0}$		CS	1
$\boldsymbol{\widetilde{f_0}}$		CS	1
$\boldsymbol{D_1}$	6.9E-2 cm^2/day	[1],[26]	1
$\boldsymbol{f_1}$		CS	0.2
$\boldsymbol{f_4}$	3.456/day	[45],[46]	2.43
$\boldsymbol{f_2}$		[25]	20
$\boldsymbol{f_3}$		CS	18
$\boldsymbol{D_3}$	1.47E-5 cm^2/day	[47]	1.7E-4
$\boldsymbol{\alpha}$	8.64E+6 cm^5 g^{-1}/day	[47]	0.1
$\boldsymbol{a_1}$		CS	0.4
$\boldsymbol{a_2}$		[25]	0.3
$\boldsymbol{F_0}$	1E-3 g cm^{-3}	[47]	1
$\boldsymbol{a_3}$	1.99E-2 /day	[48]	1.404E-2
$\boldsymbol{D_2}$		[25]	0.015
α'	8.64E+6 cm^5 g^{-1}/day	[25]	0.1
$\boldsymbol{a_0}$	0.1728 /day	[49]	0.1215
$\boldsymbol{D_4}$		[25]	1E-5
$\boldsymbol{D_5}$	1.47E-5 cm^2/day	[47]	1.7E-4
$\boldsymbol{a_4}$		[25]	1
$\boldsymbol{\beta}$	8.64E+6 cm^5 g^{-1}/day	[47]	0.1
α_5		[25]	0.675
$\boldsymbol{E_0}$	1E-3 g cm^{-3}	[50]	1

For f_0 and $\widetilde{f_0}$, they were chosen so that the debris will be digested with proper rate according to our experimental results. f_1, f_2 and f_3 were chosen so that (1) the healing process

should be consistent with the experiment; (2) their values would be comparable to which introduced in [25].

We can use the diffusion and chemotactic coefficients from Schugart [25] directly. For the coefficients on the reaction terms, however, we multiply by

$$((0.35-0.1)/0.15)^2 \approx 2.7$$

to account for the experimental design for our model that dictates an annulus wound region with outer radius of 0.35cm and the inner radius of 0.1cm as opposed to Schugart's circular wound region with radius 0.15cm.

2.4 Discussion

To quantitatively study the processes governing foreign body reactions, we have constructed a mathematical model with the capacity to predict the trends of fibroblast and macrophage population distributions, collagen or ECM accumulations by systems of partial differential equations. Our model is built based principally on biochemical mechanisms (mass action laws) and calibrated with experimental data.

Our model was modified from Schugart *et al.* [25] so that they share the common characteristic: both capturing the kinetics of inflammatory cells, fibroblasts, chemoattractant, and ECM, which are critical factors during the wound healing process. Unlike Schugart's model, we use debris cells as our inflammatory response initiator because fibrin or damaged cells are considered to be likely triggers of sub-dermal foreign body reaction. In addition, we incorporated three different phenotypes of the macrophages in our model since our focus is on the interactions between fibrotic processes and macrophage activations. We also isolate our model from angiogenic related variables at this time.

In our simulation study, we captured the need for differentiating between macrophage phenotypes because the dominance of certain phenotypes affected transient and long-term

outcomes of the healing process. When inflammatory macrophages dominated the response, the chemoattractants and other cell populations proliferated much earlier and at a higher level. Beyond its success at capturing the chemotactic and proliferation of inflammatory reaction of cells, the spatial distribution and permeability of the cells in the mathematical model simulations match well with experimental data. Therefore, the modeling study can overcome individual variances present between experimental subjects and instead present the trend of inflammatory responses.

We note that instead of remaining as constants, the proportions of different macrophage populations, λ_1, λ_2, and λ_3, are generally observed to change with time during the healing process. Macrophages are highly heterogeneous cells that can rapidly change their function in response to local environmental signals. As far as we know, there is no biomarker to identify a particular phenotype in experiments. In theory, if we have enough measurement data, we can estimate the time varying λ_1, λ_2, and λ_3. But this will be left to our future work.

At the current stage of our modeling study, the proposed model has its shortcomings. This is expected, as the complexity of the immune response system is not well understood, nor is our model sophisticated enough to include all pathways of the reactions. Nevertheless, the initial step of the modeling efforts did capture the essence of the cell and protein growth in the process, both in temporal dynamics and spatial distributions.

2.5 Stability Analysis of Two-Dimensional Model

The main mathematical contribution of this section is as follows. The non-zero equilibrium of our model represents a chronically inflamed state. If it is linearly stable in terms of the corresponding ODE system (the reactions network of the model), then it is also stable for the full system (which includes spatial diffusion and chemotaxis). In other words, spatial effects cannot de-stabilize the equilibrium if it is stable in its pure reactions. However, even if the

equilibrium is unstable by its reaction system, the spatial diffusion and chemotactic effects can help to stabilize the equilibrium under several conditions. These conditions suggest the need for the model to be dominated by classical and regulatory macrophages over the inflammatory macrophages. The mathematical proof and counter examples are given for these results.

2.5.1 Model

We conduct a stability analysis on the model presented in Chemical Kinetic Equations with Macrophage Phenotypes with the following changes made: slight changes to parameter names for clarity (i.e. $D_0 \to D_d$), MΦ cell proliferation caused by the direct interaction with chemoattractants are now assumed: $a_{11}CMH(M_0 - M),$ and lastly new experimental data shows an autocrine up-regulation of fibroblast by TGFβ without chemotaxis [51], this effect is also included in the modeling as, $a_{12}CFH(F_0 - F)$.

$$\frac{\partial D}{\partial t} = D_d \nabla^2 D - f_0 \lambda_1 MD + \tilde{f}_0 \lambda_3 M, \tag{4.6}$$

$$\frac{\partial C}{\partial t} = D_c \nabla^2 C + f_1 D + f_2 \lambda_3 M - f_3 \lambda_2 MC - f_4 C, \tag{4.7}$$

$$\frac{\partial F}{\partial t} = D_f \nabla^2 F - \chi_0 \nabla \cdot (F \nabla C) + a_1 \lambda_1 M + a_2 F \left(\frac{a_2 - a_3}{a_2} - \frac{F}{F_0} \right) + a_{12} CFH(F_0 - F), \tag{4.8}$$

$$\frac{\partial M}{\partial t} = D_m \nabla^2 M - \chi_1 \nabla \cdot (MH(M_0 - M) \nabla C) - a_0 M + a_{11} CMH(M_0 - M), \tag{4.9}$$

$$\frac{\partial E}{\partial t} = D_e \nabla^2 E - \nabla \cdot \left[\frac{BD_f}{F_0} EF \nabla F + \frac{B\chi_j}{F_0} (EFH(F_0 - F) \nabla C) \right] + a_{16} F \left(1 - \frac{E}{E_0} \right). \tag{4.10}$$

where $\nabla^2 = \nabla \cdot \nabla,$ and all coefficients are positive. The form of the logistic terms in equation (4.8) is for representing biological meanings of the coefficients.

We assume in our implant model that the computational domain is large enough and also the cell changes are slow enough (measured in days) that there is no significant boundary flux, allowing us to take homogeneous Neumann boundary conditions as a reasonable approximation.

2.5.2 Spatially Uniform Equilibria

Let us define inflammatory equilibrium as a strictly non-zero constant vector U_e in 5-dimensional space $U_e = (d_e,\ c_e, f_e, m_e, e_e)$ with $d_e > 0,\ c_e > 0,\ F_o \geq f_e > 0,\ M_o \geq m_e > 0,$ and $e_e = E_0 > 0$, which is a zero for the right hand side of the system of equations (4.6)-(4.10).

In the case of a no-flux boundary condition, the spatially uniform steady state is often used when modeling inflammatory response in tissue (see for example [38],[52]). A physically realistic, non-negative set of equilibriums can easily be obtained by letting the RHS of the original system (4.6)-(4.10) equal to zero. It is natural to define the trivial (zero) equilibrium as ground or healthy state and study its stability. Instability of the ground state is usually interpreted as unfavorable development of the disease. Here we take a different approach and are interested in analyzing the stability of the *abnormal/inflammatory* equilibrium which is non-zero for all five components of the unknown. This equilibrium can be stable or unstable depending on the parameters of the model. In this case instability of the equilibrium does not necessarily mean an unhealthy response of the immune system. An instability of a non-zero equilibrium can lead to a ground healthy state (best case scenario), to another steady state (uncertain developments), or to infinity (acute development). If in contrary, the perturbation of U_e is linearly stable, and vanishes at time infinity, then U_e can be interpreted as sustainable. All these make linear stability analysis very appealing from both a theoretical and applied point of view. It is worth mentioning that from a biological point of view, a strictly positive steady state U_e can be transition from some other non-strictly positive state. We believe that this type of interpretation of the inflammatory

equilibrium stability conditions is logical and presents an example of a sustainable wound which does not heal over the course of a long time period (see [20],[53],[54]). An indirect analogy of such an inflammatory(chronically) stable equilibrium has been introduced and applied for studying biological dynamic system in virology for some years (see [55]). At this stage of the research we are studying stability of the strictly positive state U_e mostly as a model of the inflamed equilibrium, without analysis of its genesis. As commonly occurs in biomedical research, the mathematical model can often provide non-intuitive insights into dynamics of inflammatory responses in the wound healing processes and can suggest new avenues for experimentation. In the sections to follow we determine conditions on the parameters of the system that guarantee stability of the non-zero equilibrium.

We now focus on equilibrium states that are uniform in space for this Neumann problem. By removing the spatial variations, Eqs.(4.6)-(4.10) reduce to the following ODE system:

$$\frac{dD}{dt} = -f_0\lambda_1 MD + \tilde{f}_0\lambda_3 M, \tag{4.11}$$

$$\frac{dC}{dt} = f_1 D + f_2\lambda_3 M - f_3\lambda_2 MC - f_4 C, \tag{4.12}$$

$$\frac{dF}{dt} = a_1\lambda_1 M + a_2 F\left(1-\frac{F}{F_0}\right) - a_3 F + a_{12} CFH\left(F_0 - F\right), \tag{4.13}$$

$$\frac{dM}{dt} = -a_0 M + a_{11} CMH\left(M_0 - M\right) \tag{4.14}$$

$$\frac{dE}{dt} = a_{16} F\left(1-\frac{E}{E_0}\right). \tag{4.15}$$

In looking for the equilibrium of the simplified system, Eqs.(4.11)-(4.15), we assume that our values are taken to be below threshold and therefore we ignore the Heaviside functions. There are several possible equilibrium states, but as it was pointed out earlier we focus on what one can call the interior equilibrium, one in which none of the components of the equilibrium are zero. We

let the right hand side of Eqs.(4.11)-(4.15) be zero. After some algebraic work one can obtain the following explicit formula for a unique, non-zero solution $U_e = (d_e, c_e, f_e, m_e, e_e)$:

$$
\begin{aligned}
d_e &= \frac{\tilde{f}_0 \lambda_3}{f_0 \lambda_1}, \\
c_e &= \frac{a_0}{a_{11}}, \\
e_e &= E_0, \\
m_e &= \frac{f_4 f_0 \lambda_1 a_0 - a_{11} f_1 \tilde{f}_0 \lambda_3}{f_0 \lambda_1 (f_2 \lambda_3 a_{11} - f_3 a_0 \lambda_2)}, \\
f_e &= \frac{F_0}{2a_2}\left(L_1 + \sqrt{L_1^{\,2} + 4\frac{a_2}{F_0} a_1 \lambda_1 m_e} \right).
\end{aligned}
$$

where $L_1 = a_2 - a_3 + a_{12}\left(\frac{a_0}{a_{11}}\right)$

2.5.2.1 Positivity of Equilibrium

In order for our equilibrium to be positive we find that our parameters and macrophage percentages must satisfy:

$$\frac{f_4 f_0 \lambda_1 a_0 - a_{11} f_1 \tilde{f}_0 \lambda_3}{(f_2 \lambda_3 a_{11} - f_3 a_0 \lambda_2)} > 0 \tag{4.16}$$

requiring either $f_2 \lambda_3 a_{11} > f_3 a_0 \lambda_2$,and $f_4 f_0 \lambda_1 a_0 > a_{11} f_1 \tilde{f}_0 \lambda_3$ or $f_2 \lambda_3 a_{11} < f_3 a_0 \lambda_2$,and $f_4 f_0 \lambda_1 a_0 < a_{11} f_1 \tilde{f}_0 \lambda_3$.

The condition on the parameters in inequality (4.16) says that inflammatory macrophages dominates over either regulatory or classical macrophages, and is guaranteeing existence of the inflamed steady state. This point will be expounded on further in the analysis of the conditions for stability of the non-zero equilibrium state. The illustration Figure 2-13 provides a visualization of the necessary macrophage phenotype parameter ranges. Hereafter we assume that the parameters of the original model satisfy the inequality (4.16).

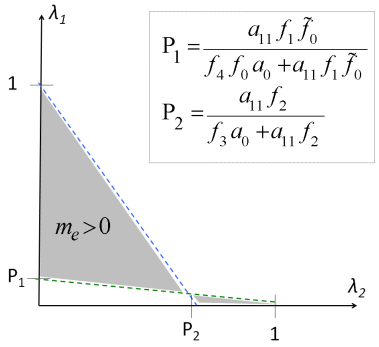

Figure 2-13 Conditions for Positive Equilibrium State

2.5.3 Linearized PDE System

Let perturbation near this equilibrium be $d = D - d_e$, $c = C - c_e$, $f = F - f_e$, $m = M - m_e$, and $e = E - e_e$ with the vector field of the perturbation denoted by $\overline{v}(x,t) = (d,c,f,m,e)$. Then the linearized system for $\overline{v}(x,t)$ will take the form

$$\frac{\partial d}{\partial t} = D_d \nabla^2 d - b_{11} d - b_{14} m \tag{4.17}$$

$$\frac{\partial c}{\partial t} = D_c \nabla^2 c - b_{21} d - b_{22} c - b_{24} m, \tag{4.18}$$

$$\frac{\partial f}{\partial t} = D_f \nabla^2 f - \chi_f \nabla^2 c - b_{32} c - b_{33} f - b_{34} m, \tag{4.19}$$

$$\frac{\partial m}{\partial t} = D_m \nabla^2 m - \chi_m \nabla^2 c - b_{42} c - b_{44} m, \tag{4.20}$$

$$\frac{\partial e}{\partial t} = D_e \nabla^2 e - \chi_{e1} \nabla^2 f - \chi_{e2} \nabla^2 c - b_{53} f - b_{55} e. \tag{4.21}$$

Where $\chi_f = f_e \chi_0$, $\chi_m = \chi_1 m_e$, $\chi_{e1} = \frac{B D_f e_0}{F_0}$, $\chi_{e2} = \frac{B \chi_j e_0 f_e}{F_0}$,

$b_{11} = f_0 \lambda_1 m_e$, $b_{14} = -(\tilde{f}_0 \lambda_3 - f_0 \lambda_1 d_e)$,

$$b_{21} = -f_1, \quad b_{22} = f_3\lambda_2 m_e + f_4, \quad b_{24} = -(f_2\lambda_3 - f_3\lambda_2 c_e),$$
$$b_{32} = -a_{12} f_e, \quad b_{33} = -\left[a_2(1 - 2\frac{f_e}{F_0}) + a_{12} c_e - a_3 \right], \quad b_{34} = -a_1\lambda_1,$$
$$b_{42} = -a_{11} m_e, \quad b_{44} = a_0 - a_{11} c_e,$$
$$b_{53} = -a_{16}(1 - \frac{e_e}{E_0}), \quad b_{55} = a_{16}\frac{f_0}{E_0}.$$

2.5.4 ODE Stability

We now focus on equilibrium states that are uniform in space for this Neumann problem. By removing the spatial variations, Eqs.(4.17)-(4.21) reduce to the following ODE system:

$$\frac{dd}{dt} = -b_{11} d - b_{14} m, \tag{4.22}$$

$$\frac{dc}{dt} = -b_{21} d - b_{22} c - b_{24} m, \tag{4.23}$$

$$\frac{df}{dt} = -b_{32} c - b_{33} f - b_{34} m, \tag{4.24}$$

$$\frac{dm}{dt} = -b_{42} c - b_{44} m \tag{4.25}$$

$$\frac{de}{dt} = -b_{53} f - b_{55} e. \tag{4.26}$$

2.5.4.1 Matrix Form

The linearized system (4.22)-(4.26) in matrix form yields:

$$\begin{bmatrix} d \\ c \\ f \\ m \\ e \end{bmatrix}' = -\mathbf{B} \begin{bmatrix} d \\ c \\ f \\ m \\ e \end{bmatrix}, \text{ where } \mathbf{B} = \begin{bmatrix} b_{11} & 0 & 0 & b_{14} & 0 \\ b_{21} & b_{22} & 0 & b_{24} & 0 \\ 0 & b_{32} & b_{33} & b_{34} & 0 \\ 0 & b_{42} & 0 & b_{44} & 0 \\ 0 & 0 & b_{53} & 0 & b_{55} \end{bmatrix}$$

For stability analysis we look at the eigenvalues of matrix $\mathbf{B}$. For convenience we rearrange our equations in the following form

$$\begin{bmatrix} m \\ d \\ c \\ f \\ e \end{bmatrix}' = \begin{bmatrix} -b_{44} & 0 & -b_{42} & 0 & 0 \\ -b_{14} & -b_{11} & 0 & 0 & 0 \\ -b_{24} & -b_{21} & -b_{22} & 0 & 0 \\ -b_{34} & 0 & -b_{32} & -b_{33} & 0 \\ 0 & 0 & 0 & -b_{53} & -b_{55} \end{bmatrix} \begin{bmatrix} m \\ d \\ c \\ f \\ e \end{bmatrix}.$$

We break $\mathbf{B}$ into a 3 block and a 2 block :

$$-\mathbf{B_1} = \begin{bmatrix} -b_{44} & 0 & -b_{42} \\ -b_{14} & -b_{11} & 0 \\ -b_{24} & -b_{21} & -b_{22} \end{bmatrix} \text{ and } -\mathbf{B_2} = \begin{bmatrix} -b_{33} & 0 \\ -b_{53} & -b_{55} \end{bmatrix}.$$

Since $\det(-\mathbf{B}-\sigma\mathbf{I}) = \det(-\mathbf{B_1}-\sigma\mathbf{I})\det(-\mathbf{B_2}-\sigma\mathbf{I})$, we find the eigenvalues by looking at the eigenvalues of the 3-block, $-\mathbf{B_1}$, and the two block, $-\mathbf{B}_2$, separately. We also simplify by noting that with the equilibrium values found above, $b_{44} = 0$ and $b_{14} = 0$ such that

$$\det[-\mathbf{B_1}-\sigma\mathbf{I}] = \begin{bmatrix} -\sigma & 0 & -b_{42} \\ 0 & -b_{11}-\sigma & 0 \\ -b_{24} & -b_{21} & -b_{22}-\sigma \end{bmatrix}$$

$$= -\sigma(b_{11}+\sigma)(b_{22}+\sigma) + b_{24}(b_{42}(b_{11}+\sigma))$$

$$= -(b_{11}+\sigma)(\sigma^2 + b_{22}\sigma - b_{24}b_{42}).$$

2.5.4.2 Eigenvalues

Solving for the roots we get the following eigenvalues:

$$\sigma_1 = -b_{11},$$

$$\sigma_2 = \frac{-b_{22} - \sqrt{(b_{22})^2 + 4b_{42}b_{24}}}{2},$$

$$\sigma_3 = \frac{-b_{22} + \sqrt{(b_{22})^2 + 4b_{42}b_{24}}}{2}.$$

The lower triangular $-\mathbf{B}_2$ gives us our final two eigenvalues:

$$\sigma_4 = -b_{33},$$
$$\sigma_5 = -b_{55}.$$

ODE stability requires the real parts $\sigma_1,...,\sigma_5$ to be negative. We proceed further to formulate the stability criteria in terms of the parameters of the model.

Under the model assumptions we have $-b_{11} < 0,\ -b_{22} < 0,\ b_{42} < 0$ and $-b_{55} < 0$.

Therefore $\sigma_1 < 0,\ \sigma_2 < 0,$ and $\sigma_5 < 0$. Next, if

$$b_{33} = a_2\left(1 - 2\frac{f_e}{F_0}\right) + a_{12}c_e - a_3 > 0, \tag{4.27}$$

then $\sigma_4 < 0.$ Finally, because $b_{42} < 0$, the real part of σ_3 is negative if and only if

$$b_{24} = -\left(f_2\lambda_3 - f_3\lambda_2 c_e\right) > 0. \tag{4.28}$$

2.5.4.3 Biological Interpretation of Stability Conditions

Assumptions in (4.27) and (4.28) have clear biological interpretations. Condition $b_{33} > 0$ requires $\left[a_2(1-2\frac{f_e}{F_0}) + a_{12}c_e < a_3\right]$ suggesting the need for the logistic growth of fibroblasts combined with the direct proliferation resulting from the presence of chemoattractants to be overcome by the death rate of fibroblasts. Condition $b_{24} > 0$ requires $f_3\lambda_2 c_e > f_2\lambda_3$ suggesting that stability is aided when the percentage of regulatory macrophages out-weighs the percentage of inflammatory macrophages.

Note that from a mathematical point of view, conditions in the form of strict inequalities imply a stronger property of the solution, namely asymptotic stability of the equilibrium. Lyapunov stability follows from the less restrictive condition with non-strict inequalities.

2.5.5 ODE Stability Implies PDE Stability

Since the interior equilibrium solution represents the inflamed state, one of the more biologically relevant questions is whether some modifications of conditions can cause the reactions to be away from the ill state, and return to healthy state. Typically the competition between diffusion and chemotaxis can aid the instability by creating spatial disturbance. One of the surprising findings for this system however, is that if the equilibrium is stable by pure reactions then it is stable for the whole reaction-diffusion-chemotactic system.

2.5.5.1 Investigating Diffusive Stability and Instability

Similar to the method Murray used [56] for determining diffusive instability (or Turing instabilities), which can cause an equilibrium from the reaction terms to become unstable under diffusion, we investigate the impact that diffusion and chemotaxis play on the stability of our full system Eqs (3.17-3.21). To start, we let

$$\overline{v}(x,t) = e^{\sigma t}\phi_{\mu_n}(x)(u_1,...,u_5) \tag{4.29}$$

be an unknown vector with five components, with separable time exponential growth and time-independent solution $\phi_n(x)$, the nth-eigenfunction for the Laplace operator with respect to the Neumann boundary conditions;

$$\begin{cases} \Delta\phi_n(x) = -\mu_n\phi_{\mu_n}(x) \text{ inside domain} \\ \dfrac{\partial\phi_{\mu_n}}{\partial n} = 0 \text{ on the boundary of the domain} \end{cases}$$

Let us for simplicity assume the domain is convex such that $\mu_n \geq 0$ for any $n \in \mathbb{N}$ is an eigenvalue for the eigenvalue problem, and ϕ_{μ_n} is its corresponding eigenfunction. We will drop the subscripts n in the text below.

Substituting the function $\overline{v}(x,t)$ in Eq.(4.29) into the linearized system Eqs.(4.17)-(4.21) yields:

$$\begin{aligned}
\sigma u_1 &= -D_d \mu u_1 - b_{11} u_1 - b_{14} u_4, \\
\sigma u_2 &= -D_c \mu u_2 - b_{21} u_1 - b_{22} u_2 - b_{24} u_4, \\
\sigma u_3 &= -D_f \mu u_3 + \chi_f \mu u_2 - b_{32} u_2 - b_{33} u_3 - b_{34} u_4, \\
\sigma u_4 &= -D_m \mu u_4 + \chi_m \mu u_2 - b_{42} u_2 - b_{44} u_4, \\
\sigma u_5 &= -D_e \mu u_5 + \chi_{e1} \mu u_3 + \chi_{e2} \mu u_2 - b_{53} u_3 - b_{55} u_5.
\end{aligned}$$

Or

$$\begin{aligned}
0 &= (\sigma + D_d \mu + b_{11}) u_1 + b_{14} u_4, \\
0 &= b_{21} u_1 + (\sigma + D_c \mu + b_{22}) u_2 + b_{24} u_4, \\
0 &= (\sigma + D_f \mu + b_{33}) u_3 - (\chi_f \mu - b_{32}) u_2 + b_{34} u_4, \\
0 &= -(\chi_m \mu - b_{42}) u_2 + (\sigma + D_m \mu + b_{44}) u_4, \\
0 &= -\chi_{e2} \mu u_2 - (\chi_{e1} \mu - b_{53}) u_3 + (\sigma + D_e \mu + b_{55}) u_5.
\end{aligned}$$

2.5.5.2 Matrix Form

Then in matrix form it takes the form

$$A(\sigma)\overline{u} = 0, \tag{4.30}$$

with matrix A defined as follows

$$\begin{bmatrix}
(\sigma + D_d \mu + b_{11}) & 0 & 0 & b_{14} & 0 \\
b_{21} & (\sigma + D_c \mu + b_{22}) & 0 & b_{24} & 0 \\
0 & -(\chi_f \mu - b_{32}) & (\sigma + D_f \mu + b_{33}) & b_{34} & 0 \\
0 & -(\chi_m \mu - b_{42}) & 0 & (\sigma + D_m \mu + b_{44}) & 0 \\
0 & -\chi_{e2} \mu & -(\chi_{e1} \mu - b_{53}) & 0 & (\sigma + D_e \mu + b_{55})
\end{bmatrix}$$

Below we will show that if the real part of all the eigenvalues of matrix $\mathbf{B}$ is negative (corresponding ODE system is stable) then non-trivial solutions of (4.30) with parameter σ having negative real part exists.

It is not difficult to see that the determinant of the matrix A has form

$$P(\sigma) = \left(\sigma + D_e\mu + b_{55}\right)\left(\sigma + D_f\mu + b_{33}\right)\det(B_1). \tag{4.31}$$

Here B_1 is a matrix associated to debris u_1, chemotaxis u_2, and macrophages u_4 parameters only;

$$\begin{bmatrix} \left(\sigma + D_d\mu + b_{11}\right) & 0 & b_{14} \\ b_{21} & \left(\sigma + D_c\mu + b_{22}\right) & b_{24} \\ 0 & -\left(\chi_m\mu - b_{42}\right) & \left(\sigma + D_m\mu + b_{44}\right) \end{bmatrix}$$

Under the assumptions that the ODE part without diffusion is asymptotically stable coefficients b_{55} and b_{33} should satisfy inequalities: $b_{44} = b_{14} = 0,\ b_{55} > 0$ and $b_{33} < 0$.

We rearrange the matrix into a (u_4, u_1, u_2)- order so that it is similar to the one addressed previously in the ODE stability analysis. Now, the characteristic equation is

$$\det[\mathbf{B_1} + \sigma\mathbf{I}] = \begin{bmatrix} \sigma + D_m\mu & 0 & b_{42} - \chi_m\mu \\ 0 & b_{11} + D_d\mu + \sigma & 0 \\ b_{24} & b_{21} & b_{22} + D_c\mu + \sigma \end{bmatrix}$$

$$= (\sigma + D_m\mu)(b_{11} + D_d\mu + \sigma)(b_{22} + D_c\mu + \sigma) - b_{24}(b_{42} - \chi_m\mu)(b_{11} + D_d\mu + \sigma)$$

$$= (b_{11} + D_d\mu + \sigma)(\sigma^2 + (b_{22} + D_c\mu + D_m\mu)\sigma + D_m\mu(b_{22} + D_c\mu) - b_{24}(b_{42} - \chi_m\mu)).$$

By solving for the roots we get the following eigenvalues:

$$\sigma_1 = -b_{11} - D_d\mu, \tag{4.32}$$

$$\sigma_2 = \frac{-(b_{22} + D_c\mu + D_m\mu) - \sqrt{(b_{22} + D_c\mu + D_m\mu)^2 + 4\epsilon}}{2}, \tag{4.33}$$

$$\sigma_3 = \frac{-(b_{22} + D_c\mu + D_m\mu) + \sqrt{(b_{22} + D_c\mu + D_m\mu)^2 + 4\epsilon}}{2}, \tag{4.34}$$

here $\epsilon = (b_{42} - \chi_m\mu)b_{24} - D_m\mu(b_{22} + D_c\mu)$.

The other two eigenvalues are:

$$\sigma_4 = -b_{33} - \mu D_f, \tag{4.35}$$

$$\sigma_5 = -b_{55} - \mu D_e. \tag{4.36}$$

We now explore explicit representations for all possible σ's focusing on the direct comparison between conditions of the stability of the linearized PDE system, (4.17)-(4.21), and the linearized ODE system, (4.22)-(4.26).

Similar to the criteria for ODE Stability, the stability for PDE requires that real parts of the all σ 's be negative.

Under the natural constraints on the parameters of our original model, $-b_{11} < 0,\ -b_{22} < 0,\ b_{42} < 0$ and $-b_{55} < 0$, we already have $\sigma_1 < 0,\ \sigma_4 < 0$ and $\sigma_5 < 0$. Therefore our criteria for PDE stability reduces to conditions:

$$b_{22} + D_c\mu + D_m\mu > 0 \text{ and } (b_{42} - \chi_m\mu)b_{24} - D_m\mu(b_{22} + D_c\mu) < 0 \tag{4.37}$$

When both of these inequalities hold we are guaranteed to have negative values for the finally two eigenvalues σ_2 and σ_3. Since stability of the ODS system forces $b_{24} > 0$ and $b_{42} < 0$, these two inequalities will be met for any $\chi_m > 0,\ D_m > 0,\ D_c > 0,\ \mu > 0$.

It follows from this argument that when the Linearized ODE system is stable then $\bar{v}(x,t)$ are converging to zero as the time goes to infinity for any eigenfunction ϕ_n. Therefore, since $\phi_n(x)$ is complete in L_2 space, one can conclude that:

The stability of the linearized PDE system (4.17)-(4.21) in L_2 space follows from the stability of the linearized ODE system, (4.22)-(4.26). We now investigate the converse statement.

2.5.6 PDE Stability Does Not Guarantee ODE Stability

As expected, the ODE stability and PDE stability are different, in this section we present one example where parameter values dictate a system which is unstable in its reaction terms ODE system, (4.22)-(4.26), but is conditionally stable in linearized PDE system (4.17)-(4.21).

Specifically we look at an example where high enough increases in macrophage chemotaxis and diffusion can overcome an instability that is rooted in its chemical reaction terms.

Let $D_m = D_c\chi_m = 0,$ then the first 5 eigenvalues of the PDE and ODE have the same sign. By definition of our original model $\sigma_1, \sigma_2,$ and σ_5 are all negative. Assume $b_{33} > 0$ (in some sense reactive terms has stabilizing effect, with respect to U_e), then $\sigma_4 < 0.$

Now if one lets $f_2\lambda_3 > f_3\lambda_2 c_e,$ which means that inflammatory macrophages dominate the regulatory macrophages, then $b_{24} < 0$ causing $\sigma_3 > 0$, and consequently the ODE system (4.22)-(4.26) is unstable. For the same set of the coefficients b's and given $\mu > 0$ it is not difficult to find sufficient condition on $D_m, D_c,$ and χ_m such that $\sigma_3 < 0,$ which guarantee stability of the equilibrium state U_e. For example, any set with the same coefficients b's with

$$D_m D_c > \frac{(b_{42} - \chi_m \mu) b_{24}}{\mu} \tag{4.38}$$

will have a real part of the $\sigma_3 < 0$ and consequently the solution of the corresponding IBVP with initial function to be $\phi_\mu(x)(u_1,...,u_5)$ will be vanishing at time infinity.

Condition (4.38) contains the following biological interpretation. Assume that inflammatory macrophages dominate the regulatory macrophages and are characterized by the coefficient

$$b_{24} = -\left(f_2\lambda_3 - f_3\lambda_2 c_e\right) < 0.$$

Then for any given value b_{24} if mobility of the macrophages and diffusion of the chemoattractant is high enough in comparison to the coefficient b_{24} then U_e is stable for the class of perturbation which corresponds to eigenfunction ϕ_μ. This example shows that Region II in Figure 2-14 is non-empty. In less strict wording, the system can be washed out if the macrophages and chemoattractant are characterized by high mobility and diffusion. This indicates vital impact

of the key parameters D_m, D_c, and χ_m on 'inflammatory' behavior (both in space and in time) of the system perturbed from equilibrium.

Obtained conclusion depend on μ and can be applied only if initial data is proportional to ϕ_μ. If in the Fourier extension of the initial data all coefficients are non-zero then the sufficient condition for stability are the same as for ODE system.

We can visualize our cases for stability as follows:

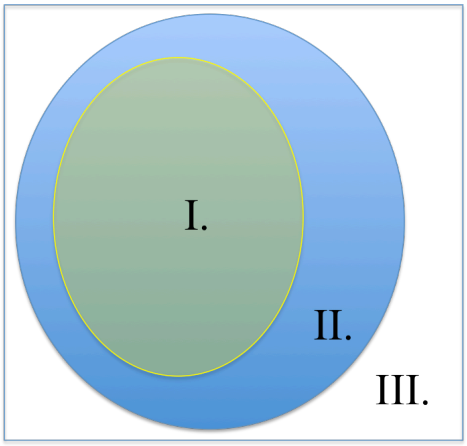

Figure 2-14 Visualization of Stability Regions for the Inflammatory Equilibrium
While not drawn to scale, this diagram helps to organize the cases for stability as we investigate conditions that will cause the inflammatory equilibrium of our system to be characterized by (I.) Linear ODE and Linear PDE stability, (II.) Instability in the ODE system but stability in the linearized PDE system, and (III.) Instability in the linearized PDE system.

In the next section we take an alternative approach to PDE Linear Analysis in order to determine a set of conditions that will produce stability of the linearized PDE system without requiring ODE Stability, yielding greater insights into Region II. of Figure 2-14.

2.5.7 Sufficient Conditions for PDE Stability

In this section we will analyze the conditional stability of the IBVP for Eq.(4.17)- (4.21) under assumption that $\overline{v}(x,t_0)$ has zero average: $\int \overline{v}(x,t_0)dx = 0.$

We will derive conditions on the coefficient of the system (4.17)-(4.21) such that the L_2 norm of the solution is bounded by the L_2 norm of the initial data, or it converges to zero at time infinity depending on the conditions on coefficients. Those conditions will depend only on coefficients of the model and Poincare constant (C_p), , which in turn depends only on the geometry of the domain.

We will also show that there exists a specific initial distribution such that the corresponding IBVP solution is vanishing at time infinity while the corresponding solution of the ODE might be unbounded at time infinity.

To aid in later simplifications, let us multiply the second through the fifth equations of the system by the percentage of classical macrophages, λ_1, and rewrite the linearized system (4.17)-(4.21) as

$$\frac{\partial d}{\partial t} = D_d \nabla^2 d - f_0 \lambda_1 m_e d - b_{14} m, \tag{4.39}$$

$$\frac{\lambda_1 \partial c}{\partial t} = \lambda_1 D_c \nabla^2 c - b_{21} \lambda_1 d - b_{22} \lambda_1 c - b_{24} \lambda_1 m, \tag{4.40}$$

$$\frac{\lambda_1 \partial f}{\partial t} = D_f \lambda_1 \nabla^2 f - \chi_f \lambda_1 \nabla^2 c - b_{32} \lambda_1 c - b_{33} \lambda_1 f - b_{34} \lambda_1 m, \tag{4.41}$$

$$\frac{\lambda_1 \partial m}{\partial t} = D_m \lambda_1 \nabla^2 m - \chi_m \lambda_1 \nabla^2 c - b_{42} \lambda_1 c - b_{44} \lambda_1 m, \tag{4.42}$$

$$\frac{\lambda_1 \partial e}{\partial t} = D_e \lambda_1 \nabla^2 e - \chi_{e1} \lambda_1 \nabla^2 f - \chi_{e2} \lambda_1 \nabla^2 c - b_{53} \lambda_1 f - b_{55} \lambda_1 e. \tag{4.43}$$

Next multiplying equations (4.39) by d, (4.40) by c, (4.41) by f, (4.42) by m, and (4.43) by e, correspondingly and integrating by parts one can easily get

$$\frac{1}{2}\frac{\partial}{\partial t}\int d^2 = -D_d\int(\nabla d)^2 - f_0\lambda_1\int d^2 - b_{14}\int md$$

$$\frac{\lambda_1}{2}\frac{\partial}{\partial t}\int c^2 = -\lambda_1 D_c\int(\nabla c)^2 - b_{21}\lambda_1\int dc - b_{22}\lambda_1\int c^2 - b_{24}\lambda_1\int mc$$

$$\frac{\lambda_1}{2}\frac{\partial}{\partial t}\int f^2 = -D_f\lambda_1\int(\nabla f)^2 + \chi_f\lambda_1\int\nabla c\nabla f - b_{32}\lambda_1\int cf - b_{33}\lambda_1\int f^2 - b_{34}\lambda_1\int mf$$

$$\frac{\lambda_1}{2}\frac{\partial}{\partial t}\int m^2 = -D_m\lambda_1\int(\nabla m)^2 + \chi_m\lambda_1\int\nabla c\nabla m - b_{42}\lambda_1\int cm - b_{44}\lambda_1\int m^2$$

$$\frac{\lambda_1}{2}\frac{\partial}{\partial t}\int e^2 = -D_e\lambda_1\int(\nabla e)^2 + \chi_{e1}\lambda_1\int\nabla f\nabla e + \chi_{e2}\lambda_1\int\nabla c\nabla e - b_{53}\lambda_1\int fe - b_{55}\lambda_1\int e^2$$

By applying the Poincare inequality,

$$C_p\int_\Omega u^2\,dx \le \int_\Omega(\nabla u)^2\,dx + \left(\int_\Omega u\,dx\right)^2,$$

to the terms $\int(\nabla u)^2 dx$ such that $C_p = C_p(\Omega) > 0,$ and adding the left and right hand sides of all 5 equations above, we group the right hand side into 10 bilinear forms which we will analyze further.

$$\begin{aligned}
&\frac{1}{2}\left[\int d^2 + \lambda_1\int\left(c^2 + f^2 + m^2 + e^2\right)\right]_t \\
&\qquad \le -\int\left[B(d,m) + B(c,d) + B(c,m) + B(c,f) + B(f,m) + B(f,e)\right] \\
&\qquad -\int\left[B(\nabla c,\nabla m) + B(\nabla c,\nabla f) + B(\nabla e,\nabla c) + B(\nabla e,\nabla f)\right] \\
&\qquad + C\left[\left(\int d\right)^2 + \left(\int c\right)^2 + \left(\int f\right)^2 + \left(\int m\right)^2 + \left(\int e\right)^2\right].
\end{aligned}$$

Where the bilinear forms are:

$$B(d,m) = 0,$$

$$B(c,d) = \lambda_1\left[\left(\frac{1}{6}D_c C_p + b_{22}\right)c^2 + b_{21}dc + (f_0 + D_d C_p)d^2\right],$$

$$B(c,m) = \lambda_1\left[\left(\frac{1}{6}D_c C_p + b_{22}\right)c^2 + b_{2,4}mc + \left(\frac{1}{3}D_m C_p + b_{44}\right)m^2\right],$$

$$B(f,m)=\lambda_1\left[\left(\frac{1}{4}D_fC_p+b_{33}\right)f^2+b_{34}cf+\frac{1}{3}D_mC_pm^2\right],$$

$$B(c,f)=\lambda_1\left[\frac{1}{6}D_cC_pc^2+b_{32}cf+\frac{1}{4}D_fC_pf^2\right],$$

$$B(f,e)=0,$$

$$B(\nabla c,\nabla m)=\lambda_1\left[\frac{1}{6}D_c(\nabla c)^2-\chi_m\nabla c\nabla m+\frac{1}{3}D_m(\nabla m)^2\right],$$

$$B(\nabla c,\nabla f)=\lambda_1\left[\frac{1}{6}D_c(\nabla c)^2-\chi_f\nabla c\nabla f+\frac{1}{4}D_f(\nabla f)^2\right],$$

$$B(\nabla f,\nabla e)=\lambda_1\left[\frac{1}{4}D_f(\nabla f)^2-\chi_{e2}\nabla f\nabla e+\frac{1}{2}D_e(\nabla e)^2\right],$$

$$B(\nabla c,\nabla e)=\lambda_1\left[\frac{1}{6}D_c(\nabla c)^2-\chi_{e1}\nabla c\nabla e+\frac{1}{2}D_e(\nabla e)^2\right].$$

We notice that this is stabilized when everything is dominated by the diffusion terms. By imposing the conditions for each bilinear form to be positive definite and using the criteria:

$$B(x,y)=ax^2+bxy+cy^2$$

is positive definite if and only if

$$a\geq 0,\ c\geq 0,\ \&\ \sqrt{ac}\geq\frac{1}{2}|b|$$

We attain 8 of the 9 conditions that are needed for PDE stability. Below we formulate a sufficient condition for the solution to be stable in L_2 space. The assumptions are presented in terms of the parameters of the original system where biological meanings are more evident.

Condition 1. If

$$\left[\left(\frac{1}{6}D_cC_p+f_3\lambda_2m_e+f_4\right)(f_0+D_dC_p)\right]^{1/2}\geq\frac{1}{2}f_1 \tag{4.44}$$

then $B(c,d)\geq 0$;

Condition 2. If

$$\left[\left(\frac{1}{4}D_f C_p - \left[a_2(1-2\frac{f_e}{F_0}) + a_{12}c_e - a_3\right]\right)\frac{1}{3}D_m C_p\right]^{1/2} \geq \frac{1}{2}a_1\lambda_1 \tag{4.45}$$

then $B(f,m) \geq 0.$

Taking into account the actual values for equilibriums: c_e, and, f_e of the inflammatory equilibrium one can reduce (4.45) to an inequality that is easier to interpret biologically. Namely, assume

$$\left[\frac{1}{4}D_f D_m C_p + \sqrt{A}D_m\right]^{1/2} \geq \frac{1}{2}a_1\lambda_1, \tag{4.46}$$

then $B(f,m) \geq 0.$ Here

$$A = \left(a_2 - a_3 + a_{12}\left(\frac{a_0}{a_{11}}\right)\right)^2 + 4\left(\frac{a_2}{F_0}\right)a_1\lambda_1\frac{f_4 f_0\lambda_1 a_0 - a_{11}f_1\tilde{f}_0\lambda_3}{f_0\lambda_1(f_2\lambda_3 a_{11} - f_3 a_0\lambda_2)}$$

Due to the assumption (4.16), parameter A is well defined for all values of the coefficients of the original model. Biological meaning of constraint (4.16) was explained in section Positivity of Equilibrium, and it is necessary for the existence of the inflamed equilibrium. What we want to point out here is that for any set of the parameters there exist large enough diffusion constants D_m, and D_f this inequality (4.46) holds, and consequently bilinear form $B(f,m) \geq 0.$

Condition 3. If

$$\begin{aligned}&\left[\left(\frac{1}{6}D_c C_p + (f_3\lambda_2 m_e + f_4)\right)\left(\frac{1}{3}D_m C_p + (a_{11}m_e - a_0)\right)\right]^{1/2} \\ &\quad \geq \frac{1}{2}\left|f_2\lambda_3 - f_3\lambda_2 c_e\right|\end{aligned} \tag{4.47}$$

then $B(c,m) \geq 0.$ To insure the RHS in (4.47) is well-posed, assume that

$$\left(\frac{1}{3}D_m C_p + (a_{11}m_e - a_0)\right)$$
$$= \frac{1}{3}D_m C_p + a_{11}\frac{f_4 f_0 \lambda_1 a_0 - a_{11} f_1 \tilde{f}_0 \lambda_3}{f_0 \lambda_1 (f_2 \lambda_3 a_{11} - f_3 a_0 \lambda_2)} - a_0 \geq 0. \tag{4.48}$$

We rewrite the above inequality in terms of the parameters of the original model to point out that for any given set of the parameters there exists big enough coefficient D_m, characterizing macrophages mobility, such that inequality (4.47) holds.

Condition 4. If

$$\left[\frac{1}{6}D_c C_p \frac{1}{4}D_f C_p\right]^{1/2} \geq \frac{1}{2}a_{12} f_e, \tag{4.49}$$

then $B(c, f) \geq 0$.

Condition 5. If

$$\left(\frac{1}{6}D_c \frac{1}{3}D_m\right)^{1/2} \geq \frac{1}{2}\chi_m \tag{4.50}$$

then $B(\nabla c, \nabla m) \geq 0$.

Condition 6. If

$$\left(\frac{1}{6}D_c \frac{1}{4}D_f\right)^{1/2} \geq \frac{1}{2}\chi_f \tag{4.51}$$

then $B(\nabla c, \nabla f) \geq 0$.

Condition 7. If

$$\left(\frac{1}{4}D_f \frac{1}{2}D_e\right)^{1/2} \geq \frac{1}{2}\chi_{e2} \tag{4.52}$$

then $B(\nabla f, \nabla e) \geq 0$.

Condition 8. If

$$\left(\frac{1}{6}D_c\frac{1}{2}D_e\right)^{1/2} \geq \frac{1}{2}\chi_{e1} \tag{4.53}$$

then $B(\nabla c, \nabla e) \geq 0$.

We now assume that spatial averages for all five components $d(x,0), c(x,0), f(x,0), m(x,0),$ and $f(x,0)$ are equal 0 (Initial data are orthogonal to 1). Then due to no-flux Neumann condition on the boundary,

$$\int_\Omega d = 0; \int_\Omega c = 0; \int_\Omega f = 0; \int_\Omega m = 0; \int_\Omega e = 0, \tag{4.54}$$

Since we are studying linear stability these will stay zero for $t > 0$. Under these Conditions (1-8), Lyapunov stability of the linearized system is guaranteed. Furthermore, if we add the assumption that the inequalities on (4.44)-(4.49) then the system will be asymptotically stable, and the L_2 norm of the solution will exponentially converge to zero as time goes to infinity.

2.5.7.1 Significance of Sufficient Conditions for PDE Stability

In all above eight conditions inequalities hold for big enough values of diffusive coefficients. This highlights the importance of the spatial distribution of the perturbation for the equilibrium. The major meaning of these conditions is that for any set of the parameters if diffusivity coefficients are big enough then U_e is stable. Another key parameter, which characterizes the behavior of the spatial distribution of the system is the chemotactic coefficient. We now set out to gain additional quantitative insight into the chemotactic coefficient for macrophage cells and investigate how its relation to these diffusion coefficients can affect on stability. This is done by comparing two inequalities, one produced through eigenvalue analysis

for specific parameters, and the other taken directly from cond.(5) above. We do not assume the ODE stability conditions of the equilibrium in this section.

It will be easy to construct a spatially inhomogeneous solution of the Initial-Boundary Value Problem (IBVP) so that the solution of corresponding ODE for $V = \int \bar{v}(x,t)dx$ is identically zero, where the PDE solutions can be either stable or unstable by adjusting certain parameters.

Indeed, let the domain be the segment $[0,\pi]$ and as in Eq.(4.29) with $\phi = cosx$. Then in order for $v(x,t)$ to be a solution of corresponding IBVP it is necessary and sufficient that σ be a root of the characteristic polynomial equation $P(\sigma)$ in Eq. (4.31).

To establish that Cond.(1-8) are essential, we show an example of the system with: (1) Cond.(1-8) all met, and (2) $P(\sigma)$ has a positive root in Eq. (4.31). For the selected domain we assume Poincare constant $C_p = 1$. We begin our construction by assuming coefficients satisfy the inequalities in constraints Cond.(1-8) except for Cond.(3) and Cond.(5).

Let $b_{22} \geq 4/5D_c$, $a_{11}m_e \geq a_0$ and $0 > b_{24} \geq -\left(D_c D_m / 20\right)^{1/2}$. Obviously for these set of the parameter, Cond.(3) is satisfied. Then if $\sqrt{D_c D_m / 60} \geq \chi_m$, Cond.(5) holds and consequently $v(x,t) \to 0$ as $t \to \infty$.

Furthermore, it is not difficult to see that if $b_{22} = 4/5D_c$, and $b_{24} = -\left(D_c D_m / 20\right)^{1/2}$ then σ_2 in Eq. (4.33) is positive provided:

$$(\chi_m - b_{42})\left[\frac{D_c D_m}{20}\right]^{1/2} - \frac{9}{5}D_m D_c > 0. \tag{4.55}$$

This inequality holds if

$$\chi_m > \sqrt{102 D_c D_m}. \tag{4.56}$$

Consequently, when Inequality (4.56) holds then $\| v(x,t) \|_{L_2} \to \infty$ as $t \to \infty$.

Comparing stability in (4.50) and instability when inequality (4.56) is satisfied, provides us with a way to highlight the impact of the diffusive constants and chemotactic coefficients on the stability of the inflamed equilibrium U_e. From the example above one can see that if the chemotactic sensitivity coefficient χ is relatively bigger than the diffusivity characteristic of the process then U_e is unstable. At the same time if it is relatively smaller, as in inequalities (4.50)-(4.53) then the inflamed equilibrium is stable.

2.6 Discussion

To further study the processes governing inflammatory and fibrotic reactions against foreign bodies, we have taken our mathematical model, expressed by a system of partial differential equations with no flux boundary conditions, and have considered a biologically meaningful equilibrium state of the system and its stability conditions.

We have provided a mathematical proof that when this equilibrium is stable in the corresponding ODEs, then it is also stable for the full system in $L^2(\Omega)$. These conditions correspond with feasible biological conditions where the percentage of regulatory macrophages dominate that of the inflammatory macrophages. However a system with a parameter set can be conditionally stable in the PDE sense when its ODE system is not necessarily stable. We provided some exclusive conditions for this to happen.

We mention here that the system has infinitely many equilibria, all except for one contain at least one zero component. The one under discussion here is called the interior equilibrium as it has 5 non-zero components. This particular equilibrium corresponds to an inflamed state of the healing process, whose instability is an indicator of three possible dynamics: 1. Best case scenario-returning to the healthy state; 2. Uncertain development - transition to another 'abnormal' equilibrium; 3. Acute inflammatory response (worst case scenario) perturbations tend to infinity.

Our main mathematical results indicate that the inflamed state's stability mainly depends on the reaction dynamics. We found that even in the case where spatial diffusion is small and chemotactic affects are large we cannot achieve de-stabilize of an equilibrium that is stable in the reaction-only system. On the other hand, if the equilibrium is unstable by its reaction-only system, then spatial diffusion over chemotactic effects can help to stabilize the equilibrium if the initial perturbation is subjected to specific constraints.

Chapter 3

Stem Cell Influence on Model

Fibrotic encapsulation is often attributed to the over-activity of certain immune cells. Many experiments have been dedicated to investigating this challenge and many innovative changes to implant surface properties have been proposed. Changes to the surface texture, the hydrophilic properties, as well as coating the implant with various cells/proteins have shown to impact the anchoring capability of the implant as well as the scaring and inflammation [57]. A growing interest in experimentation has been in increasing the availability of stem cells at the wound site [29].

In this chapter we propose an expanded mathematical model (4.6)-(4.10), a set of 8 partial differential equations, adapted from mass-action laws by the principles of wound healing and analyze it to gain insights regarding the dynamics of immune cells and proteins following the insertion of a foreign body. Specifically we focus on the impact of mesenchymal stem cells on inflammation and fibrosis.

Furthermore we test the model's accuracy and investigate the roles stem cells play on the components of our system. We focus our attention on the equilibrium family that represents a healed state, one in which the macrophage populations return to zero but varying amounts of mast cell activation remain. We determine the conditions that must be met by the stem cell population in order to affect the early population trend of regulatory macrophages (specifically to change the monotonicity from decreasing to increasing). This shows that through chemical reactions alone stem cell presence can help create a better environment for healing.

3.1 Modeling Based on Chemical Kinetics

As we seek to analyze the effects that stem cell presence can play on fibrotic reactions we again take the lead from the modeling techniques for wound healing used by Schugart [25] as discussed in section 2.1 above but we make several new adjustments:

- Mast Cells are assumed to be the initiators of the immune responses and prompt an up-regulation of Pro-Inflammatory Cytokines through the release of histamine.
- Cytokines are divided into two classifications, Regulatory and Pro-Inflammatory, these classifications not only help specify their roles but also establish an association to the macrophage phenotypes that promote them.
- Classical macrophages can be grouped in with Inflammatory macrophages classification because they share in the same reactions to cytokines and stem cells.
- A distinction between Regulatory and Inflammatory macrophages is important because they are recruited by different cytokines and are affected by the presence of mesenchymal stem cells in different ways (i.e. stem cells suppress inflammatory macrophages while promoting regulatory macrophages).
- Mesenchymal Stem Cells (described in section 1.2.8 maintain stem cell qualities after proliferation, and are also influenced by a death rate.

Figure 3-1 provides an overview of these biological considerations and the chemical interactions that are important when incorporating Mesenchymal Stem Cell influence into foreign body responses.

Combining several modeling principles that have been applied to wound healing models, along with the several experimentally observed impacts of stem cells on key immune cells. We take a simplified approach to stem cell modeling by assuming an absence of differentiation stimuli (as done experimentally in [58]), and therefore isolate the ability of stem cell presence to promote the up-regulation of regulatory macrophages, meanwhile inhibiting inflammatory macrophage

population growth (as is consistent with the findings of [28]). We also take a simplified death rate of stem cells (as modeled in [40]) but also account for the experimentally observed proliferation in which the divided cells continue to maintain stem cell qualities [30].

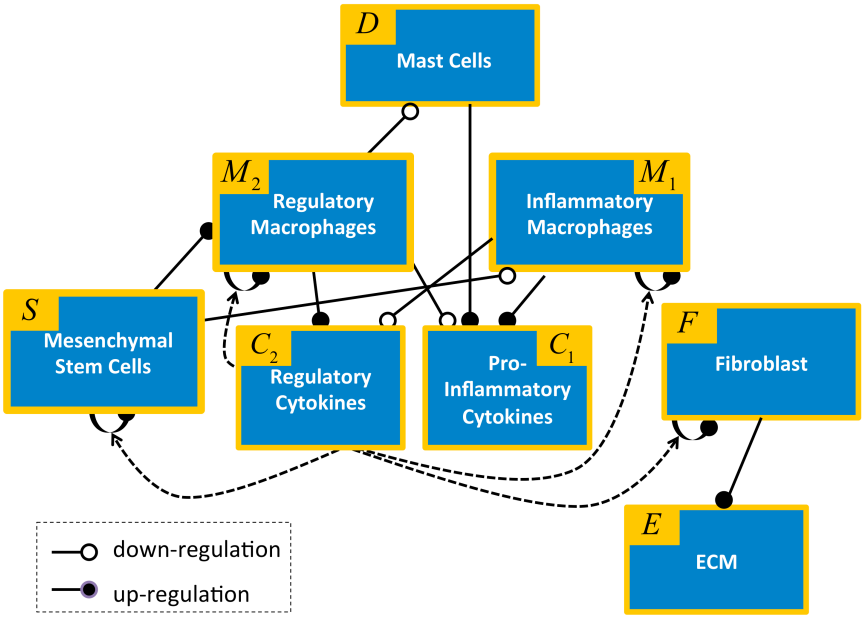

Figure 3-1 Reaction Schematic with MSC:
This schematic summarizes the biological reaction between the cells and cytokines included in modeling foreign body responses with mesenchymal stem cell influences.

In addition to the reaction terms that account for the up-regulation and down-regulation of each component we also include cell migration and chemotaxis (consistent with Schugart [25]). In efforts to look closely at the effects of stem cell and macrophage variations on tissue recovery in a manageable mathematical setting we leave oxygen pressure and angiogenic details out at this moment. Our foreign body fibrotic reaction model is:

$$\frac{\partial D}{\partial t} = D_d \nabla^2 D - f_0 M_2 D, \tag{5.1}$$

$$\frac{\partial C_1}{\partial t} = D_c \nabla^2 C_1 + f_1 D + f_2 M_1 - f_3 M_2 C_1 - f_4 C_1, \tag{5.2}$$

$$\frac{\partial C_2}{\partial t} = D_c \nabla^2 C_2 + f_5 M_2 - f_6 M_1 C_2 - f_4 C_2, \tag{5.3}$$

$$\frac{\partial F}{\partial t} = D_f \nabla^2 F - \chi_0 \nabla \cdot (F \nabla C_2) + a_2 F \left(\frac{a_2 - a_3}{a_2} - \frac{F}{F_0} \right) + a_{12} C_2 F H_f, \tag{5.4}$$

$$\frac{\partial M_1}{\partial t} = D_m \nabla^2 M_1 - \chi_1 \nabla \cdot (M_1 H_m \nabla C_1) - a_0 M_1 + a_{11} C_2 M_1 H_m - a_{18} S M_1, \tag{5.5}$$

$$\frac{\partial M_2}{\partial t} = D_m \nabla^2 M_2 - \chi_1 \nabla \cdot (M_2 H_m \nabla C_2) - a_0 M_2 + a_{11} C_2 M_2 H_m + a_{19} S M_2, \tag{5.6}$$

$$\frac{\partial S}{\partial t} = D_m \nabla^2 S - \chi_2 \nabla \cdot (S \nabla C_2) - a_{21} S + a_{20} S C_2, \tag{5.7}$$

$$\frac{\partial E}{\partial t} = D_e \nabla^2 E - \nabla \cdot \left(\frac{B D_f}{F_0} E F \nabla F + \frac{B \chi_j}{F_0} (E F H_f \nabla C_2) \right) + a_{16} F \left(1 - \frac{E}{E_0} \right). \tag{5.8}$$

Where $\nabla^2 = \nabla \cdot \nabla$, $H_m = H(M_0 - (M_1 + M_2))$, and $H_f = H(F_0 - F)$, H is the Heaviside function, and all coefficients are positive.

For the above system (5.1)-(5.8) the cell population D represents activated mast cells. We assume that mast cell activation decreases in proportion to the amount of $M_2 -$ regulatory macrophages and mast cells present at the implant site. Spatial diffusion of the mast cell population is also accounted for, $D_d \nabla^2 D$.

As mentioned previously in this section, we separate the chemical interactions that drive immune response into two separate components: pro-inflammatory cytokines, C_1 and regulatory cytokines, C_2.

Pro-inflammatory cytokines, C_1, which includes histamine are released both by inflammatory macrophages M_1 as well as during degranulation of activated mast cells, but are

inhibited by M_2 - regulatory macrophage cells. The diffusion of these cytokines in space is accounted for through $D_c\nabla^2 C_1$.

Regulatory cytokines, C_2 consist mainly of interleukin-4 and various growth factors, including Tissue Growth Factors type beta (TGFβ), which serve to drive cell proliferation, blood vessel growth and recruitment of macrophages of the regulatory phenotype. These cytokines are released by regulatory macrophages and inhibited by inflammatory macrophages M_1. The diffusion of these cytokines $D_c\nabla^2 C_2$ is assumed to share the same diffusion coefficient D_c as the inflammatory cytokines.

Fibroblast density, F, are up-regulated by the cytokines C_2 which promote proliferation and collagen synthesis. Thus fibroblast population F and the extracellular matrix E can be modeled in the same manner as in our previous model (4.10).

Macrophage population is divided up into two classes dependent on phenotype, M_1 - inflammatory macrophages, and M_2 - regulatory macrophages. Both populations share the same proliferation (caused by a direct interaction with C_2) and decay rates, but they are recruited by different cytokines and are affected by the presence of mesenchymal stem cells in different ways. Stem cells suppress inflammatory macrophages while promoting regulatory macrophages. M_1 and M_2 density redistribution through diffusion and chemotactic drift is up-regulated by the corresponding chemotactic gradient fields C_1 and C_2, respectively. Furthermore we account for the carrying capacity of the space so that productions reach a limiting value once the combined macrophage populations reach a saturation of M_0.

Similar to regulatory macrophages, mesenchymal stem cell density S is also modeled to incorporate diffusion and chemotactic-drift up-regulated by the C_2 chemotactic gradient field.

Additionally proliferation of the stem cells due to direct interaction with C_2 and cell apoptosis is incorporated.

We refer Table 3-1 to for a detailed list of the roles and values assigned to the reaction term coefficients of this model.

Furthermore, for our model we assume that the computational implant domain is large enough and that changes in cell movement are slow enough (being measured in days) that flux along the boundary becomes insignificant, allowing homogeneous Neumann boundary conditions to be assumed.

3.1.1 Spatially Uniform Equilibrium States

We seek a family of equilibria that are uniform in space for this Neumann boundary problem. Removing the spatial variation reduces our system to:

$$\frac{dD}{dt} = -f_0 M_2 D, \tag{5.9}$$

$$\frac{dC_1}{dt} = f_1 D + f_2 M_1 - f_3 M_2 C_1 - f_4 C_1, \tag{5.10}$$

$$\frac{dC_2}{dt} = f_5 M_2 - f_6 M_1 C_2 - f_4 C_2, \tag{5.11}$$

$$\frac{dF}{dt} = a_2 F\left(\frac{a_2 - a_3}{a_2} - \frac{F}{F_0}\right) + a_{12} C_2 F H_f, \tag{5.12}$$

$$\frac{dM_1}{dt} = -a_0 M_1 + a_{11} C_2 M_1 H_m - a_{18} S M_1, \tag{5.13}$$

$$\frac{dM_2}{dt} = -a_0 M_2 + a_{11} C_2 M_2 H_m + a_{19} S M_2, \tag{5.14}$$

$$\frac{dS}{dt} = -a_{21} S + a_{20} S C_2, \tag{5.15}$$

$$\frac{dE}{dt} = a_{16} F\left(1 - \frac{E}{E_0}\right). \tag{5.16}$$

We assume that our values are taken to be below threshold and therefore take $H_f = H_m = 1$ as we determine equilibria for the system above. Many equilibrium states exist, we chose to analyze the family of equilibria in which the ECM has reached its threshold value and the concentrations of both phenotypes of macrophages, as well as stem cell concentrations return to zero. We classify this family as "healed states" owning to the disappearance of these inflammatory cells after the wound is healed. This class was observed as a limiting solution for a large class of initial conditions in ode simulations conducted on this system, and is able to capture expected biological behaviors and give us further insights about the roles of stem cell on our system.

By taking the RHS of the system above to be equal zero one can obtain a system of 8 nonlinear equations, which can be explicitly solved. After some algebraic work one can obtain the following formula for the family of positive equilibrium states $U_e = (d_e, c_{1e}, c_{2e}, f_e, m_{1e}, m_{2e}, s_e, e_e)$ that represent a healed state:

$$d_e = \text{free}, \tag{5.17}$$

$$c_{1e} = \left(\frac{f_1}{f_4}\right) d_e, \tag{5.18}$$

$$c_{2e} = 0, \tag{5.19}$$

$$f_e = (F_0 / a_2)\left[a_2 - a_3 + a_{12}\left(\frac{a_{21}}{a_{20}}\right)\right], \tag{5.20}$$

$$m_{1e} = 0, \tag{5.21}$$

$$m_{2e} = 0, \tag{5.22}$$

$$s_e = 0, \tag{5.23}$$

$$e_e = E_0, \tag{5.24}$$

Conditions for the existence of this family of equilibria of positive components are as follows:

$$d_e \geq 0,$$
$$a_2 + a_{12}\left(\frac{a_{21}}{a_{20}}\right) \geq a_3.$$

These conditions are easily met as fibroblast growth, a_2 is widely accepted to be greater than its death rate, a_3 during healing processes [59].

3.1.2 Linearized System

Let the perturbation near this equilibrium be $d = D - d_e, c_1 = C_1 - c_{1e}, c_2 = C_2 - c_{2e}$, $f = F - f_e$, $m_1 = M_1 - m_{1e}$, $m_2 = M_2 - m_{2e}$, $s = S - s_e$, $e = E - e_e$. Denote vector field of the perturbation by $\overline{v}(x,t) = (d, c_1, c_2, f, m_1, m_2, s, e)$, then the linearized system for $\overline{v}(x,t)$ is:

$$\frac{\partial d}{\partial t} = D_d \nabla^2 d - b_{11} d - b_{16} m_2, \tag{5.25}$$

$$\frac{\partial c_1}{\partial t} = D_c \nabla^2 c_1 - b_{21} d - b_{22} c_1 - b_{25} m_1 - b_{26} m_2, \tag{5.26}$$

$$\frac{\partial c_2}{\partial t} = D_c \nabla^2 c_2 - b_{33} c_2 - b_{35} m_1 - b_{36} m_2, \tag{5.27}$$

$$\frac{\partial f}{\partial t} = D_f \nabla^2 f - \chi_f \nabla^2 c_2 - b_{43} c_2 - b_{44} f, \tag{5.28}$$

$$\frac{\partial m_1}{\partial t} = D_m \nabla^2 m_1 - \chi_{m1} \nabla^2 c_1 - b_{53} c_2 - b_{55} m_1 - b_{57} s, \tag{5.29}$$

$$\frac{\partial m_2}{\partial t} = D_m \nabla^2 m_2 - \chi_{m2} \nabla^2 c_2 - b_{63} c_2 - b_{66} m_2 - b_{67} s, \tag{5.30}$$

$$\frac{\partial s}{\partial t} = D_m \nabla^2 s - \chi_s \nabla^2 c_2 - b_{73} c_2 - b_{77} s, \tag{5.31}$$

$$\frac{\partial e}{\partial t} = D_e \nabla^2 e - \chi_{e1} \nabla^2 f - \chi_{e2} \nabla^2 c_2 - b_{84} f - b_{88} e. \tag{5.32}$$

Here the parameters are

$$\chi_f = f_e\chi_0,\ \chi_{m1} = \chi_1 m_{1e},\ \chi_{m2} = \chi_1 m_{2e},$$
$$\chi_s = \chi_2 s_e,\ \chi_{e1} = \frac{BD_f e_0 f_e}{F_0},\ \chi_{e2} = \frac{B\chi_f e_0 f_e}{F_0},$$
$$b_{11} = f_0 m_{2e},\ b_{16} = f_0 d_e,$$
$$b_{21} = -f_1,\ b_{22} = f_3 m_{2e} + f_4,\ b_{25} = -f_2,\ b_{26} = f_3 c_{1e},$$
$$b_{33} = f_6 m_{1e} + f_4,\ b_{35} = f_6 c_{2e},\ b_{36} = -f_5,$$
$$b_{43} = -a_{12} f_e,\ b_{44} = -\left[a_2(1 - 2\frac{f_e}{F_0}) + a_{12} c_{2e} - a_3 \right],$$
$$b_{53} = -a_{11} m_{1e},\ b_{55} = -a_{11} c_{2e} + a_{18} s_e + a_0,\ b_{57} = a_{18} m_{1e},$$
$$b_{63} = -a_{11} m_{2e},\ b_{66} = a_0 - a_{11} c_{2e} - a_{19} s_e,\ b_{67} = -a_{19} m_{2e},$$
$$b_{73} = -a_{20} s_e,\ b_{77} = -a_{20} c_{2e} + a_{21},$$
$$b_{84} = -a_{16}(1 - \frac{e_e}{E_0}),\ b_{88} = a_{16}\frac{f_e}{E_0}.$$

3.2 Stability Analysis of ODE System

Turning now to take a look at the stability of the system we find the linearized system of our reaction terms to be:

$$\frac{dd}{dt} = -b_{11} d - b_{16} m_2, \tag{5.33}$$

$$\frac{dc_1}{dt} = -b_{21} d - b_{22} c_1 - b_{25} m_1 - b_{26} m_2, \tag{5.34}$$

$$\frac{dc_2}{dt} = -b_{33} c_2 - b_{35} m_1 - b_{36} m_2, \tag{5.35}$$

$$\frac{df}{dt} = -b_{43} c_2 - b_{44} f, \tag{5.36}$$

$$\frac{dm_1}{dt} = -b_{53} c_2 - b_{55} m_1 - b_{57} s, \tag{5.37}$$

$$\frac{dm_2}{dt} = -b_{63} c_2 - b_{66} m_2 - b_{67} s, \tag{5.38}$$

$$\frac{ds}{dt} = -b_{73} c_2 - b_{77} s, \tag{5.39}$$

$$\frac{de}{dt} = -b_{84} f - b_{88} e. \tag{5.40}$$

In matrix form, $\left[(d,c_1,c_2,f,m_1,m_2,s,e)^T\right]' = -\mathrm{B}\cdot(d,c_1,c_2,f,m_1,m_2,s,e)^T$ where **B** is:

$$\mathbf{B} = \begin{bmatrix} b_{11} & 0 & 0 & 0 & 0 & b_{16} & 0 & 0 \\ b_{21} & b_{22} & 0 & 0 & b_{25} & b_{26} & 0 & 0 \\ 0 & 0 & b_{33} & 0 & b_{35} & b_{36} & 0 & 0 \\ 0 & 0 & b_{43} & b_{44} & 0 & 0 & 0 & 0 \\ 0 & 0 & b_{53} & 0 & b_{55} & 0 & b_{57} & 0 \\ 0 & 0 & b_{63} & 0 & 0 & b_{66} & b_{67} & 0 \\ 0 & 0 & b_{73} & 0 & 0 & 0 & b_{77} & 0 \\ 0 & 0 & 0 & b_{84} & 0 & 0 & 0 & b_{88} \end{bmatrix}.$$

For stability analysis of the healed state equilibria we look at the eigenvalues of matrix $-\mathbf{B}$. For convenience we rearrange our equations in the following order $(d,m_2,s,c_2,m_1,c_1,f,e)^T$ and take advantage of Eq.(5.17)-(5.24), which give $b_{11}=0, b_{35}, b_{53}, b_{57}, b_{63}, b_{67}, b_{73},$ and $b_{84}=0$:

$$\left[\begin{array}{cc|cccccc} 0 & b_{16} & 0 & 0 & 0 & 0 & 0 & 0 \\ 0 & b_{66} & 0 & 0 & 0 & 0 & 0 & 0 \\ \hline 0 & 0 & b_{77} & 0 & 0 & 0 & 0 & 0 \\ 0 & b_{36} & 0 & b_{33} & 0 & 0 & 0 & 0 \\ 0 & 0 & 0 & 0 & b_{55} & 0 & 0 & 0 \\ b_{21} & b_{26} & 0 & 0 & b_{25} & b_{22} & 0 & 0 \\ 0 & 0 & 0 & b_{43} & 0 & 0 & b_{44} & 0 \\ 0 & 0 & 0 & 0 & 0 & 0 & 0 & b_{88} \end{array}\right] = \begin{bmatrix} \mathbf{B_1} & 0 \\ 0 & \mathbf{B_2} \end{bmatrix}.$$

Since $\det(-\mathbf{B}-\sigma\mathbf{I}) = \det(-\mathbf{B_1}-\sigma\mathbf{I})\det(-\mathbf{B_2}-\sigma\mathbf{I})$, we find the eigenvalues by looking at the eigenvalues of the 2-block, $-\mathbf{B_1}$, and the 6-block ,$-\mathbf{B_2}$, separately.

$$\begin{aligned} \det[-\mathbf{B_1}-\sigma\mathbf{I}] &= \begin{bmatrix} -\sigma & -b_{16} \\ 0 & -b_{66}-\sigma \end{bmatrix} \\ &= -\sigma(-b_{66}-\sigma) \end{aligned}$$

giving us the following eigenvalues:

$$\begin{aligned} \sigma_1 &= 0, \\ \sigma_2 &= -b_{66}. \end{aligned}$$

The lower triangular $-\mathbf{B_2}$ gives us our final six eigenvalues:

$$\begin{aligned}\sigma_3 &= -b_{77},\\ \sigma_4 &= -b_{33},\\ \sigma_5 &= -b_{55},\\ \sigma_6 &= -b_{22},\\ \sigma_7 &= -b_{44},\\ \sigma_8 &= -b_{88}.\end{aligned}$$

ODE exponential stability requires the real parts of the $\sigma_1,...,\sigma_8$ to be negative. The constraints of our model (i.e. the assumption that parameter values are positive) give us:

$$\begin{aligned}-b_{66} < 0, -b_{77} < 0, -b_{33} < 0, -b_{55} < 0,\\ -b_{22} < 0, -b_{44} < 0, \text{and} -b_{88} < 0.\end{aligned}$$

Therefore, $\sigma_2,...,\sigma_8$ are always negative, so we have negative eigenvalues corresponding to all components except the free component of our equilibrium, σ_1 which is zero. Thus we need to further investigate the full nonlinear system. Our non-negative equilibrium comes from the mast cell term, D, in our matrix.

This makes the mast cell, D, component our main focus as we further investigate the nonlinear stability of the system Eq.(5.33)-(5.40).

3.2.1 Non-Linear Convergence of B1 Block

Since the mast cell (D) is coupled only with M_2 in our model, we begin to analyze the stability of these two components:

$$\begin{aligned}\frac{dD}{dt} &= -f_0 M_2 D,\\ \frac{dM_2}{dt} &= -a_0 M_2 + a_{11} C_2 M_2 H_m + a_{19} S M_2.\end{aligned}$$

We extract the equilibrium, keep the non-linear terms, and account for simplification due to the zero equilibrium terms (specifically m_{2e}, s_e and c_{2e}) yielding the following ODEs:

$$d' = -b_{16}m_2 - f_0 m_2 d,$$
$$m_2' = -a_0 m_2 + a_{11}c_2 m_2 + a_{19}s m_2.$$

Looking first at m_2, we can divide by m_2 and solve:

$$m_2(t) = m_2(0)e^{\int_0^t (a_{11}c_2 + a_{19}s - a_0)ds}.$$

Furthermore, since we observed that the eigenvalues in B_2 are negative we know that s and c_2 will remain within a small neighborhood about 0. By setting $a_{11}c_2 \le \frac{1}{4}a_0$ and $a_{19}s \le \frac{1}{4}a_0$. We now have

$$m_2(t) \le m_2(0)e^{-\frac{1}{2}a_0 t}. \tag{5.41}$$

This bound for m_2 gives us the exponential bound for this component. We use this bound to help us as we investigate d. We rewrite the d component ODE in the following way:

$$d' + f_0 m_2 d = -b_{16}m_2$$

We solve by multiplying by the integral factor yielding:

$$\left(e^{\int_0^t f_0 m_2(\eta)d\eta}\right)d' + \left(e^{\int_0^t f_0 m_2(\eta)d\eta}\right)\left(f_0 m_2 d\right) = \left(e^{\int_0^t f_0 m_2(\eta)d\eta}\right)\left(-b_{16}m_2\right),$$
$$\frac{d}{dt}\left[\left(e^{\int_0^t f_0 m_2(\eta)d\eta}\right)d(t)\right] = \frac{-b_{16}}{f_0}\cdot\frac{d}{dt}\left(e^{\int_0^t f_0 m_2(\eta)d\eta}\right),$$
$$\int_0^t \left(d(\tau)e^{\int_0^\tau f_0 m_2(\eta)d\eta}\right)' d\tau = \frac{-b_{16}}{f_0}\cdot\int_0^t \left(e^{\int_0^\tau f_0 m_2(\eta)d\eta}\right)' d\tau,$$
$$d(t)e^{\int_0^t f_0 m_2(\eta)d\eta} - e^0 d(0) = \frac{-b_{16}}{f_0}\left[e^{\int_0^t f_0 m_2(\eta)d\eta} - e^0\right],$$
$$d(t) = \frac{-b_{16}}{f_0} + \left(d(0) + \frac{b_{16}}{f_0}\right)e^{-\int_0^t f_0 m_2(\eta)d\eta}.$$

Furthermore, by Eq. (5.41),

$$\int_0^t f_0 m_2(s)ds \to \text{constant as } t \to \infty \text{ because}$$

Cauchy Criterion holds, by letting $M = ln\left(\frac{K_1}{\epsilon}\right)$ then for every

$$\epsilon > 0 \text{ and } t_2 > t_1 \geq M$$

$$\text{we have} \int_{t_1}^{t_2} |m_2(s)ds| \leq m_2(0) \int_{t_1}^{t_2} e^{-\frac{1}{2}a_0 s}\, ds \leq K_1 \left(e^{-\frac{1}{2}a_0 t_1} - e^{-\frac{1}{2}a_0 t_2} \right) \leq \epsilon$$

$$\text{where } K_1 = \frac{2m_2(0)}{a_0}$$

We now have that $d(t)$ converges as t approaches infinity and this convergence itself exhibits exponential decay. So, while we have freedom to move between different equilibrium states within the family (not being forced to return to the same mast cell value) of equilibrium are stable as long as:

$$\lim_{t\to\infty}(a_{11}C_2 + a_{19}S - a_0) < 0.$$

Therefore, this family of equilibria are shown to be stable. However, even though small perturbations still return to the family, as we observed they do not necessarily return to the same mast cell (D) initial value. We conduct further investigation to discover how the presence of stem cells affect both the asymptotic limit of mast cell (D) as well as the transient behavior of the system.

3.3 Stability Analysis of Linearized PDE System

To investigate whether stability in the system can persist under chemotaxis and diffusion, we investigate whether any Turing instability exists in Eq.(5.25)-(5.32) with respect to the Neumann boundary conditions. Let $\overline{v}(x,t) = e^{\sigma t}\phi_n(x)(u_1,...,u_8)$ be a vector with eight unknown components:

$$\begin{cases} \Delta\phi_n(x) = -\mu_n\phi_n(x) \text{ inside domain} \\ \dfrac{\partial\phi_n}{\partial n} = 0 \text{ on the boundary of the domain} \end{cases}$$

where $\phi_n(x)$, a time-independent function, is an eigenfunction for Δ corresponding to the eigenvalue $\mu_n > 0$ (we assume a convex domain for simplicity). Substituting $\overline{v}(x,t)$ into the linearized PDE system gives:

$$\begin{aligned}
\sigma u_1 &= -D_d \mu_n u_1 - b_{11} u_1 - b_{16} u_6, \\
\sigma u_2 &= -D_c \mu_n u_2 - b_{21} u_1 - b_{22} u_2 - b_{25} u_5 - b_{26} u_6, \\
\sigma u_3 &= -D_c \mu_n u_3 - b_{33} u_3 - b_{35} u_5 - b_{36} u_6, \\
\sigma u_4 &= -D_f \mu_n u_4 + \chi_f \mu_n u_3 - b_{43} u_3 - b_{44} u_4, \\
\sigma u_5 &= -D_m \mu_n u_5 + \chi_{m1} \mu_n u_2 - b_{53} u_3 - b_{55} u_5 - b_{57} u_7, \\
\sigma u_6 &= -D_m \mu_n u_6 + \chi_{m2} \mu_n u_3 - b_{63} u_3 - b_{66} u_6 - b_{67} u_7, \\
\sigma u_7 &= -D_m \mu_n u_7 + \chi_s \mu_n u_3 - b_{73} u_3 - b_{77} u_7, \\
\sigma u_8 &= -D_e \mu_n u_8 + \chi_{e1} \mu_n u_4 + \chi_{e2} \mu_n u_3 - b_{84} u_4 - b_{88} u_8.
\end{aligned}$$

We add the right hand side over to the left and recall that at the equilibrium of interest, $b_{11}, b_{35}, b_{53}, b_{57}, b_{63}, b_{67}, b_{73}, b_{84}, \chi_{m1}, \chi_{m2}$, and χ_s equal zero. The following matrix form $\mathbf{A}(\sigma)\overline{u} = \mathbf{0}$ with $\overline{u}$ is rearrange to $\overline{u} = (u_1, u_6, u_7, u_3, u_5, u_2, u_4, u_8)^T$ results,

$$\mathbf{A} = \begin{pmatrix} \mathbf{A_1} & \mathbf{0} \\ \mathbf{A_3} & \mathbf{A_2} \end{pmatrix}.$$

Where

$$\mathbf{A_1} = \begin{pmatrix} (\sigma + D_d \mu_n) & b_{16} \\ 0 & (\sigma + D_m \mu_n + b_{66}) \end{pmatrix},$$

$$\mathbf{A_2} = \begin{pmatrix} d_{s,7} & 0 & 0 & 0 & 0 & 0 \\ 0 & d_{c,3} & 0 & 0 & 0 & 0 \\ 0 & 0 & d_{m,5} & 0 & 0 & 0 \\ 0 & 0 & b_{25} & d_{c,2} & 0 & 0 \\ 0 & (-\chi_f \mu_n + b_{43}) & 0 & 0 & d_{f,4} & 0 \\ 0 & -\chi_{e2} \mu_n & 0 & 0 & -\chi_{e1} \mu_n & d_{e,8} \end{pmatrix},$$

and $\mathbf{A_3} = \begin{pmatrix} 0 & 0 \\ 0 & b_{36} \\ 0 & 0 \\ b_{21} & b_{26} \\ 0 & 0 \\ 0 & 0 \end{pmatrix}$ where $d_{x,\alpha} = \sigma + D_x\mu_n + b_{\alpha\alpha}$.

In the previous section we showed that the determinant of $\mathbf{B_2}$ had eigenvalues with negative real parts. We now investigate if these eigenvalues maintain a negative real part now that chemotactic and diffusion terms are taken into account. We again break down the determinant of $\mathbf{A}$ by isolating the determinant of the 2-block, $\mathbf{A_1}$ and the 6-block, $\mathbf{A_2}$. The upper triangular property of $\mathbf{A_1}$ gives us that:

$$\sigma_1 = -D_d\mu_n,$$
$$\sigma_2 = -b_{66} - D_m\mu_n.$$

Furthermore, since $\mathbf{A_2}$ is lower triangular (just as $\mathbf{B_2}$ was in the ODE case) solving the determinant we find:

$$\sigma_3 = -b_{77} - D_s\mu_n,$$
$$\sigma_4 = -b_{33} - D_c\mu_n,$$
$$\sigma_5 = -b_{55} - D_m\mu_n,$$
$$\sigma_6 = -b_{22} - D_c\mu_n,$$
$$\sigma_7 = -b_{44} - D_f\mu_n,$$
$$\sigma_8 = -b_{88} - D_e\mu_n$$

It is easily seen that, under the assumption that the eigenvalues of the ODE system have negative real part, diffusion terms help, rather than disrupt, the sustaining of negative σ values in the linearized PDE system.

We see that, for Neumann boundary conditions, no Turing instability exists and conclude that our equilibrium, which was found to be stable in the ODE system, will maintain its stability as

we extend the system to include the diffusion and chemotactic properties of the cell/protein populations in our model.

3.4 Investigation of Free Component of Equilibrium

With the freedom of our system to move between steady states that vary in the mast cell population level (and consequently C_1 level) under small perturbations we now look closer at the reaction system to determine what terms affect the value for which D converges to.

Looking at the ODE reactions:

$$\frac{dD}{dt} = -f_0 M_2 D,$$

dividing by D, applying the chain rule to $\ln D$ with respect to t allows us to substitute then integrate to attain the solution:

$$D(t) = D(0)e^{\int_0^t -f_0 M_2(s)ds}$$

where $D(0)$ is the initial condition on $D(t)$ at time zero. Observing that D depends on the integral behavior of M_2, more specifically behaving as a decreasing function of M_2. We see M_2, holds the key to increase or decrease activated mast cell (D) populations. To determine what leads to higher M_2 we look now at Eq. (5.14) by a similar technique.

$$\frac{dM_2}{dt} = -a_0 M_2 + a_{11} C_2 M_2 + a_{19} S M_2,$$

Again we can divide by and solve for $M_2(t)$:

$$M_2(t) = M_2(0)e^{\int_0^t (a_{11}C_2 + a_{19}S - a_0)dt}$$

where $M_2(0)$ is the initial value of $M_2(t)$ at time zero. We let

$$\lim_{t\to\infty}(a_{11}C_2 + a_{19}S - a_0) \le 0$$

which will achieve the desired asymptotic behavior of M_2. Additionally we see that increases in C_2 and S have the ability to increase M_2 which as noted above decreases D. This implies that, while stem cell coating may not change the stability of the family of equilibrium, it can help drive the system to a lower mast cell (D) component at steady state which is representative of healing with less inflammation.

3.5 Transient Behavior of ODE System

Simulations of solutions to the ODE system at varied stem cell initial values led to an assertion that stem cell presence at the time of implantation can affect the monotonicity of some of the key cell populations in the system. Since C_2 and M_2 help to mediate healing and prevent uncontrolled inflammation it is important for overall healing that these terms increase in population during the beginning stages of healing processes. We investigate the conditions under which these two components can be made to increase assuming the equilibrium state to be in the family detailed above.

$$\frac{dM_2}{dt} = -a_0 M_2 + a_{11} C_2 M_2 H_m + a_{19} S M_2$$

Assuming we are under the macrophage threshold, we take H_m to be one. In order for M_2 to be increasing we need $\frac{dM_2}{dt} > 0$ which is achieved when:

$$(a_{11} C_2 + a_{19} S) M_2 > a_0 M_2, \text{ i.e.}$$
$$a_{11} C_2 + a_{19} S > a_0.$$

Here we see the direct impact of the stem call on the ability for M_2 to satisfy the condition for being an increasing function.

$$\frac{dc_2}{dt} = f_5 m_2 - (f_6 m_{1e} + f_4) c_2 - f_6 c_{2e} m_1,$$

When equilibrium values $m_{1e} = 0, m_{2e} = 0, c_{2e} = 0$ are accounted for, our investigation into the C_2 transient behavior yields:

$$\frac{dC_2}{dt} = f_5 M_2 - f_4 C_2.$$

Now we see that C_2 will be increasing when $\frac{dC_2}{dt} > 0$ which occurs when

$$M_2 > \frac{f_4 C_2}{f_5}.$$

Greater values of M_2 make this inequality easier to attain which is consistent with the assertion that stem cell coating can help switch C_2 to be increasing in nature at the beginning of the healing process as it increases the M_2 population.

3.5.1.1 Simulation Confirms Initial Stem Cell Influences Monotonicity of Macrophage

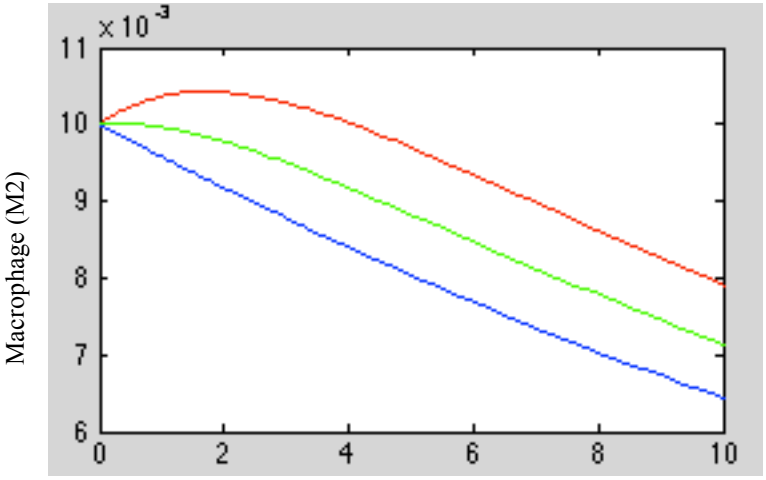

Figure 3-2 Initial Behavior of M_2 for Varied Initial MSC Amounts: bottom line (blue) denotes the system with no stem cell coating, the middle line (green) an initial coating of .5, and the top line (red) an initial coating of 1. Under our parameter set regulatory macrophages are increasing initially before decaying when the initial stem cell coating is high enough.

These finding are consistent with the transient behavior seen in the simulation of Eq. (5.9)-(5.16). Simulations were conducted using Matlab ode15s under specified initial condition and the parameter values in Table 3-1.Simulation is provided in Figure 3-2. Under our parameter set $\frac{dM_2}{dt} > 0$ as long as $S(0) > 0.42$.

3.6 Model Simulation Compared with Experimental Data

We further test the ability of the computational model to capture the outcomes consistent with different experimental settings. Rather than directly coating a biomedical devise with MSCs investigation is being conducted as to the costs and benefits of instead introducing a stem cell recruiter to the implant site.

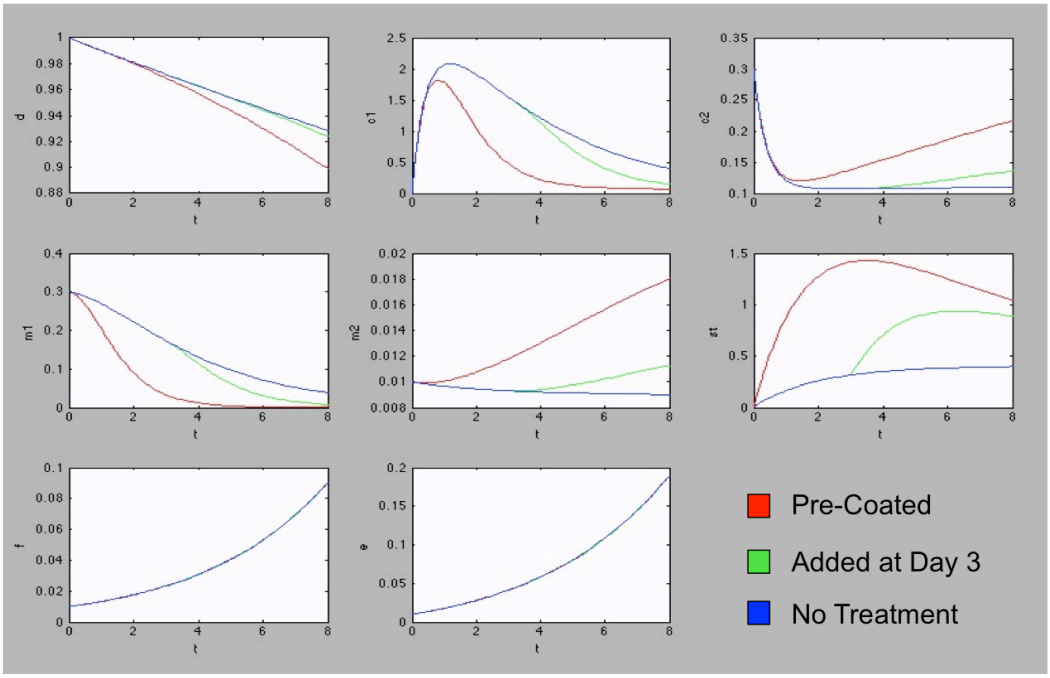

Figure 3-3 Temporal Dynamics Influenced by Stem Cell Recruitor Treatments
Matlab simulation of reaction terms of model, Eqs.(5.9)-(5.16), where control is taken such that a natural influx of stem cell, "+r_0", is assumed and added to Eq.(5.15). SDF D0 is characterized by an additional recruitment term "+r_1e^(-r_2t)" in which r_1= 1 and r_2= 0.2. SDF D3 is characterized by a similar recruitment set to initiate at t=3 days, "+(r_3e^(-r_2(t-3))H(t-3)" where r_3= 0.5 and r_2=0.2.

We adapt our model slightly to better emulate a stem cell recruiter and compare our results with the experimental findings of Thevenot et al. published 2010 [28]. The only change is that stem cell equation has a source term due to the recruiter. Temporal Dynamics of the effects of Stem Cell recruitor on the cell populations in our system are shown in Figure 3-3.

We investigate two cases in which Stromal Derived Factor-1 alpha (SDF-1α) a chemokine documented to serve as a recruiter for stem cell migration is introduced into the implant domain. Under one treatment plan, SDF D0, the implant scaffold is pre-coated with a SDF-1α solution and in the second treatment plan, SDF D3, an injection of SDF-1α is delivered via injection directly to the implant site 3 days after surgery. Figure 3-4 documents the previously recorded experimental findings from [28] as well as the results for our model to compare the MSC cell density a week after surgery. Figure 3-5 compares the Macrophage cell density at this same time step. Our cell population values are computed from Eqs. (5.9)-(5.16), with additional source term, using Matlab and account only for the reaction terms of our model.

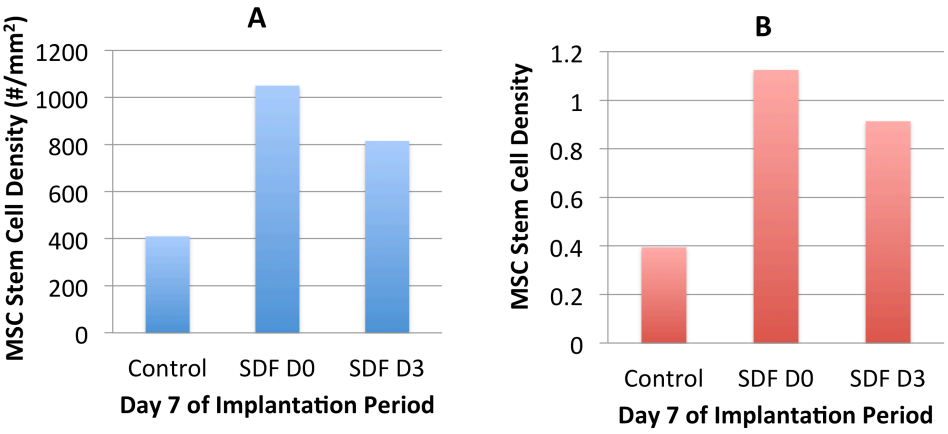

Figure 3-4 Stem Cell Density Results
Control represents the cell density after no treatment, SDF D0 represents pre-implantation scaffold coating of SDF-1α, and SDF D3 corresponds to a single injection of SDF-1α 3 days post surgery. (A) Experimental data for the MSC stem cell density come from the number of SSEA-4+CD45- cells per mm^2 as recorded in [28] (B) Stem Cell Densities from Simulation presented in Figure 3-3 at t=7.

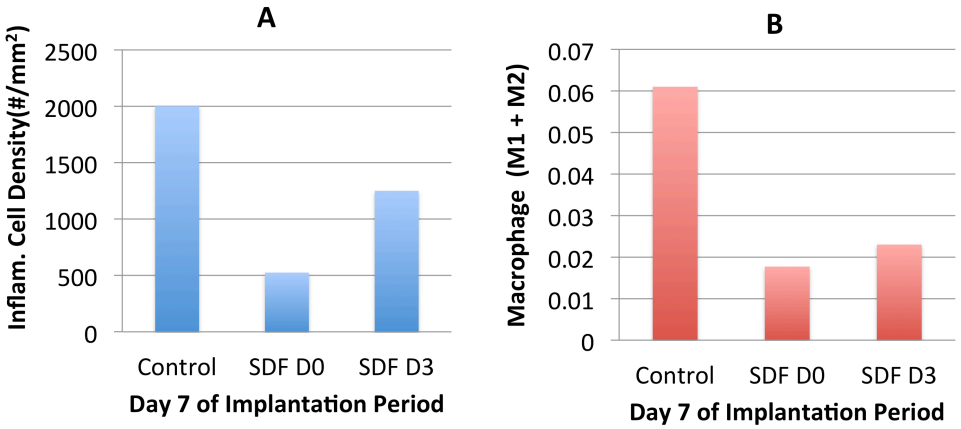

Figure 3-5 Macrophage Cell Density Results:
with same experimental (A) and computational modeling (B) settings as in Figure 3-4 . Here Macrophage densities from the model are taken to be the sum of the inflammatory M_1 and regulatory M_2 cell populations.

Figure 3-4 and Figure 3-5 help confirm the applicability of our model. The proportionate affects that treatments plans SDF D0 and SDF D3 had on the MSC population (Figure 3-4) are consistent with the predictions of our model. Our model does show some discrepancy in the effects of these treatments on the Macrophage population (Figure 3-5). The overall behavior is captured, the largest macrophage population occurring in the control case, Second largest population occurring under the SDF D3 plan, and the smallest macrophage population being observed when the implant was pre-coated with stem cell recruiters (treatment SDF D0). Our model, however, when considering the SDF D3 relative to the control case predicted a steeper decline in macrophage population then what was actually observed in the experimental data. This is not surprising though and stem cells from our choice to account only for cellular reactions in our computer simulation. Cell migration and chemotaxis are not yet accounted for in our computational simulations and will likely help account for the under approximation of macrophage-cell densities seen for treatment plan SDF D3 in Figure 3-5 .

3.6.1 Parameter Values

The majority of our mathematical analysis is done without specified parameters. This allows for the flexibility to adapt the model for different implant types and different hosts and allows us to reach conclusions that can be more broadly applied.

In order to better visualize the ODE system we established a set of parameters for the system (See Table 3-1). They are rooted in the parameters estimated by Schugart [25] but adjusted under criteria found in several other publications.

Table 3-1 Parameters for Reaction Terms of Stem Cell Incorporated Model
here "CS" refers to parameter values unique to this Current Study

Parameter	Description	Value	Reference
f_0	Regulatory macrophage suppression of activated mast cells	1	[41]
f_1	Mast cell secretion of cytokines	0.2	CS
f_2	Inflammatory macrophage up-regulation of inflammatory cytokines	20	[25]
f_3	Suppression of inflammatory cytokines by regulatory macrophages	18	[41]
f_4	Decay of cytokines	2.43	[25]
f_5	Regulatory macrophage up-regulation of regulatory cytokines	30	[25]
f_6	Suppression of regulatory cytokines by inflammatory macrophages	1	CS
a_2	Proliferation of fibroblast	0.3	[25]
a_3	Death rate of fibroblast	0.01404	[25]
a_0	Death rate of macrophages	0.045	[25]
a_{16}	Growth of ECM	0.675	[25]
a_{18}	Suppression of inflammatory macrophages by stem cells	0.7	CS
a_{19}	Up-regulation of regulatory macrophages by stem cells	0.1	CS
a_{20}	Proliferation of stem cells due to regulatory cytokines	0.08	[30]
a_{21}	Decay of stem cell (due to apoptosis or differentiation)	0.5	[40]
a_{12}	Direct proliferation of fibroblast due to cytokines	0.001	CS
a_{11}	Direct proliferation of macrophage due to cytokines	0.01	[35]
F_0	Fibroblast threshold	1	[25]
E_0	ECM threshold	1	[25]
M_0	Macrophage threshold	1	[25]

3.7 Discussion

The effects of stem cells on wound healing processes has become of growing interest. Many have found evidence to support that stem cells help create a better atmosphere for recovery, but the avenues by which this influence occurs are widely theorized and debated. Many believe stem cell influence to be carried out through a second monocyte-derived cell which has recently (1994) adopted the name Fibrocyte [60] and others focus on the stem cell ability to speed up angiogenesis [61] thereby filling in wound gaps and bringing greater avenues for white blood cells to migrate to the wound site. In this chapter, with goals set specifically to glean more insight into stem cell influence on macrophage populations, we chose not to account for angiogenesis and instead isolated the pure interactions that stem cells play with other key immune regulators. We propose an expanded model in Appendix A, a model that incorporates Fibrocytes as a variable in the PDE system, but we do not conduct analysis on this model at this time.

We have concluded mathematically that the Stem Cell population can have a direct impact on both the early behavior of regulatory macrophages and the long term healing outcome. By choosing an approach where simulations are isolated to the reaction terms, our approach resembles an in-vitro experimental setting over in-vivo setting in the way that blood vessel growth is not accounted for.

Specifically we determine the long term conditions that must be met by the stem cell population in order for the healthy state to remain stable, and also the early conditions on the stem cell population that are needed in order to positively affect the early population trend of regulatory macrophages, specifically to change the monotonicity from decreasing to increasing. This shows that through chemical reactions alone, stem cell presence can help create a better environment for healing. We refer to [35] for an in-depth look at how an increased macrophage population of the regulatory profile early in the wound healing process can mean the difference between whether or not long term healing is achieved.

Chapter 4

Conclusion

In Chapter 1 the biological setting of sub-dermal cellular response to foreign bodies was presented. We looked at mathematical techniques for modeling population dynamics and specifically investigated our Modified Dale model, which extends the wound healing, reaction-diffusion model by Dale et al. [32]. This investigation highlighted the positive effects of incorporating Macrophage in wound healing models, specifically within the sub-dermal foreign body response context.

In Chapter 2 we constructed a new model, a system of five PDEs, which modifies the wound-healing model by Schugart *et al.*[25]. The model is based principally on biochemical mechanisms (mass-action laws) and calibrated with experimental data to capture key components of wound healing: the kinetics of inflammatory cells, fibroblasts, chemoattractant, and ECM. Unlike Schugart's model, we used debris cells as our inflammatory response initiator because fibrin or damaged cells are considered to be likely triggers of sub-dermal foreign body reaction. In addition, we incorporated three different phenotypes of the macrophages in our model. This is done to focus is on the interactions between fibrotic processes and macrophage activations, a main goal in our research pursuits. Our modeling considerations also isolated the healing processes from angiogenic related variables. Beyond its success at capturing the chemotactic and proliferation of inflammatory reaction of cells, the spatial distribution and permeability of the cells in the mathematical model simulations matched well with experimental data. Therefore, the modeling study can overcome individual variances present between experimental subjects and instead present the trend of inflammatory responses.

We then investigated the stability of this system of partial differential equations assuming no-flux boundary conditions and find that the inflammatory state's stability mainly depends on the reaction dynamics. We provided a mathematical proof that when the inflammatory (interior)

equilibrium is stable in the corresponding ODEs, then it is also stable for the full PDE system in $L^2(\Omega)$. We investigated the converse and found a counterexample showing that if the equilibrium is unstable by its reaction-only system, then spatial diffusion over chemotactic effects can stabilize the equilibrium if the initial perturbation is subjected to specific constraints.

The need for distinction to be made between macrophage phenotypes when investigating fibrotic response is made evident by both our simulation study and our stability analysis because the dominance of certain phenotypes were shown to affect the transient and long-term outcomes of the healing process. In simulations, when inflammatory macrophages dominated the response, the chemoattractants and other cell populations proliferated much earlier and at a higher level. In stability analysis we found that the biological conditions for the inflamed equilibrium to be characterized by stability required the percentage of regulatory macrophages dominate that of inflammatory macrophage.

In Chapter 3 we extended our model to a system of 8 partial differential equations. This model focused on the effects that stem cell presence has on healing processes. Another key addition we made to the model is in separating the Chemoattractant term into two classifications, regulatory and pro-inflammatory. We also treated macrophage phenotypes as unique variables, they could no longer be assumed to share the same governing equation because stem cell presence has been show to affect the phenotypes in distinct ways. We tested the temporal dynamics of this model against the results found in our collaborating bioengineering lab, Thevenot et al [28]. Experimentally, three different stem cell related treatment plans were tested and our simulation study was found to agree with the findings.

Analytically we studied the stability of the healthy equilibria, which was identified as a family of equilibria where macrophage components return to zero. We determined the long term conditions that must be met by the stem cell population in order for the healthy state to remain stable, and also the early conditions on the stem cell population that are needed in order to

positively affect the early population trend of regulatory macrophages, specifically to change the monotonicity from decreasing to increasing. This shows stem cell presence can help create a better environment for healing even when chemical reactions alone are accounted for.

In the appendix we present an extended model from the one presented in Chapter 3 and include fibrocyte cell influence. Full analysis on this model has yet to be conducted.

The use of mathematical models in bioengineering study has several advantages. First, our results support that this model can be used to investigate multiple variables and complex interactions in a systematic way, thereby supplementing experimental results. Second, these models can be modified to simulate different types of inflammatory and fibrotic diseases; a study that would otherwise be very difficult to achieve through experiments methods. Finally, by further developing mathematical models, we will, with greater confidence, be able to use them to identify the critical parameters and timing for the treatment/intervention needed in order to alter fibrotic tissue reactions toward favored outcomes.

As experimental data and research of foreign body fibrotic reactions continue there are several areas were further investigation into the areas of this dissertation can be extended and improved.

1. The impacts of stem cell involvement on post implant healing is quite vast, there are several consequences of stem cell presence that our model cannot yet capture. So far, we have only captured what the stem cells affect on inflammatory mediators. There is a need to further include the impact stem cells have on promoting angiogenesis, and on suppressing Fibrocytes [40], [61]. Continued experimental data from the bioengineering lab would help us further validate both parameter values and distinctions between macrophage phenotypes. As it stands, Thevenot [28] investigated the effects of stem cell recruiters (introduced according to different treatment plan timings) on fibrotic response, but their macrophage cell counts were collected without distinction by phenotypes. While we were still able to compare our model simulation accuracy by

combining our Macrophage phenotypes together, acquiring experimental data where macrophage cell counts were separated by phenotype would allow us to closer examine the accuracy of our model in capturing the correct separated macrophage densities.

2. Restricting our stability analysis to the constraints of Neumann Boundary Conditions does not allow us to assess quantitative outcomes in the case when flux from blood vessels is accounted for. We will enforce a mixed boundary condition to better capture the migratory processes of key cells and proteins from nearby blood vessels. We have begun work to include mixed boundary conditions on the model in Chapter 2. The impact of the new boundary conditions has not been investigated in full, but in current stage it appears manageable in eigenvalue problem analysis. We take the interior boundary, Γ_{in}, to model the migration behavior from a nearby blood vessel. We take the exterior boundary, Γ_{ex}, to model the migration from nearby tissue, refer to Figure 4-1.

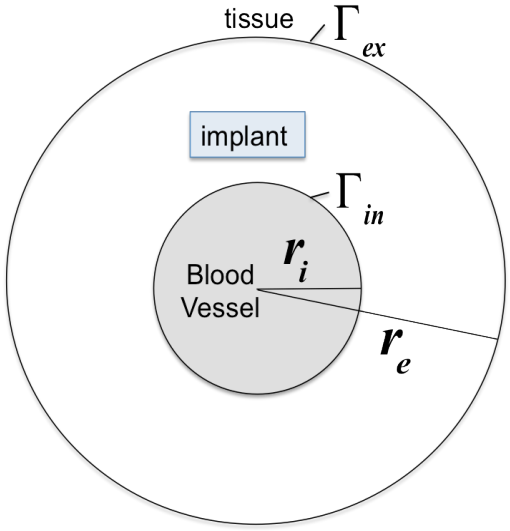

Figure 4-1 Implant in Relation to New Boundary Considerations
New boundary conditions for the foreign body response model presented in chapter 2 can help us to identify the change in stability when flux of inflammatory regulators across the inner boundary are permitted.

We let both interior and exterior boundary conditions for the debris term, D, take Neumann boundary conditions under the assumption that this term originates purely from the implant process itself. Migration of chemoattractants from the blood into the implant domain is taken to be promotional to the amount at which the Chemoattractant in the domain exceeds that of the normal concentration in the blood. The interior boundary migration of the Macrophage population is taken to be proportional to the chemoattractant population and is set to shut off when either the macrophage threshold is reached or the chemoattractant concentration fails to be higher than the normal chemoattractant level in the blood. Similarly we assume Fibroblast migration to have the same dependence as that of Macrophages; dependent on the chemoattractant level with programmed shut off at Fibroblast threshold. We assume that ECM is produced purely by the cells at the implant site and therefore takes on Neumann boundary conditions on both boundaries. Additionally we take Neumann boundary conditions for all terms on the exterior boundary assuming the migration is originating purely from the site of the blood vessel on the inner boundary.

Inner Boundary, Γ_{in}, conditions:

$$\nabla D \cdot \mathbf{n}\big|_{\Gamma_{in}} = 0$$

$$\nabla C \cdot \mathbf{n}\big|_{\Gamma_{in}} = -b_c(C - C_{av})$$

$$\nabla M \cdot \mathbf{n}\big|_{\Gamma_{in}} = b_m(C - C_{av})H(M_0 - M)$$

$$\nabla F \cdot \mathbf{n}\big|_{\Gamma_{in}} = b_f(C - C_{av})H(F_0 - F)$$

$$\nabla E \cdot \mathbf{n}\big|_{\Gamma_{in}} = 0$$

where $\mathbf{n}$ is the normal vector and C_{av} is the normal, maintained level of chemoattractant in the blood. Exterior Boundary Γ_{ex} is taken to have Neumann boundary conditions.

We analyze the Eigenvalue Problem with Mixed Boundary Conditions and investigate the degree to which stability conditions must be violated in order for instability to occur. Under a small adjustment to the chemotactic consideration for Macrophages, we have found it analytically possible to isolate conditions that can be used to produce an instability of the healed equilibrium state (as represented in the sign of the eigenvalue), and will continue our work expecting to find that flux terms can aid the stability of the healed equilibrium state.

In summary, we have presented mathematical models in this dissertation and shown their valuable as theoretical tools for the simulating foreign body reaction processes. With further refinement we aim to capture a more complete picture of stem cell influence and use the model to continue to gain insights into potential causes of fibrosis that lead to implant failure as well as to isolate key parameters and timing that can give direction to treatment plans to promote both short and long term implant success.

Appendix A
Fibrocyte Role in Foreign Body Response: An Additional Model

Fibrocyte cells and their roles in foreign body fibrotic reactions are still widely disputed. The recent focus on fibrosis has led to the discovery of the Fibrocyte. A cell with bone marrow origin that is thought to be an intermediary cell that contributes to the Macrophage and Fibroblast concentrations. It is believed that interleukin influences Fibrocytes to differentiate into macrophages that fit a classical profile[60]. While TGFβ, on the other hand, causes fibrocytes differentiate into myofibroblasts in dermal wound healing experiments [62]. In the following system we propose a new model that includes this newly discovered Fibrocyte cell, F_1.

$$\frac{\partial D}{\partial t} = D_d \nabla^2 D - f_0 M_2 D, \tag{6.1}$$

$$\frac{\partial C_1}{\partial t} = D_c \nabla^2 C_1 + f_1 D + f_2 M_1 - f_3 M_2 C_1 - f_4 C_1, \tag{6.2}$$

$$\frac{\partial C_2}{\partial t} = D_c \nabla^2 C_2 + f_5 M_2 - f_6 M_1 C_2 - f_4 C_2, \tag{6.3}$$

$$\frac{\partial F_1}{\partial t} = D_F \nabla^2 F_1 - \nabla(\chi_0 F_1 \nabla C_2) - a_3 F_1 - f_7 C_1 F_1 - f_8 C_2 F_1 - a_{17} S F_1, \tag{6.4}$$

$$\frac{\partial F_2}{\partial t} = D_f \nabla^2 F_2 - \nabla(\chi_0 F_2 \nabla C_2) + a_2 F_2 (1 - F_2 / F_0) - a_3 F_2 + f_9 C_2 F_1, \tag{6.5}$$

$$\frac{\partial M_1}{\partial t} = D_m \nabla^2 M_1 - \nabla(\chi_m H_m M_1 \nabla C_1) - a_0 M_1 + a_{11} C_2 M_1 H_m + f_{10} C_1 F_1 - a_{18} S M_1, \tag{6.6}$$

$$\frac{\partial M_2}{\partial t} = D_m \nabla^2 M_2 - \nabla(\chi_m H_m M_2 \nabla C_2) - a_0 M_2 + a_{11} C_2 M_2 H_m + a_{19} S M_2, \tag{6.7}$$

$$\frac{\partial S}{\partial t} = D_m \nabla^2 S - \nabla(\chi_s S \nabla C) + a_{20} C_2 S - a_{21} S, \tag{6.8}$$

$$\frac{\partial E}{\partial t} = \nabla(D_E \nabla E + \frac{B D_f E}{F_0} \nabla F_2 - \frac{B \chi_f E F_2}{F_0} H(F_0 - F_2) \nabla C_2) + a_{16} F_2 (1 - \frac{E}{E_0}). \tag{6.9}$$

Where $\nabla^2 = \nabla \cdot \nabla$, $H_m = H(M_0 - (M_1 + M_2))$, and H is the Heaviside function, and all coefficients are positive. We incorporates those two experimentally observed features: the loss of Fibrocytes as they become fibroblasts, F_2, in proportion to TGFβ represented by C_2, and the loss of fibrocytes as they become Classical Macrophages, a subset of M_1, in proportion to interleukin, a Pro-

Inflammatory Cytokine expressed as C_1. Furthermore stem cell presence, S, is suspected to suppress fibrocyte populations, so this too is included in the reaction terms of the modeling. Since parameters and scaled effects of fibrocytes are still widely disputed it is difficult to know with certainty which parameters should be chosen when running numerical simulations. We do however provide a Matlab simulation, Figure 4-2, with preliminary results showing the temporal dynamics of Eqs.(6.1)-(6.9) for three specified initial stem cell concentrations. The lack of a positive source term for the Fibrocyte population presents temporal dynamics of similar behavior to when Fibrocytes were excluded in Chapter 3 model.

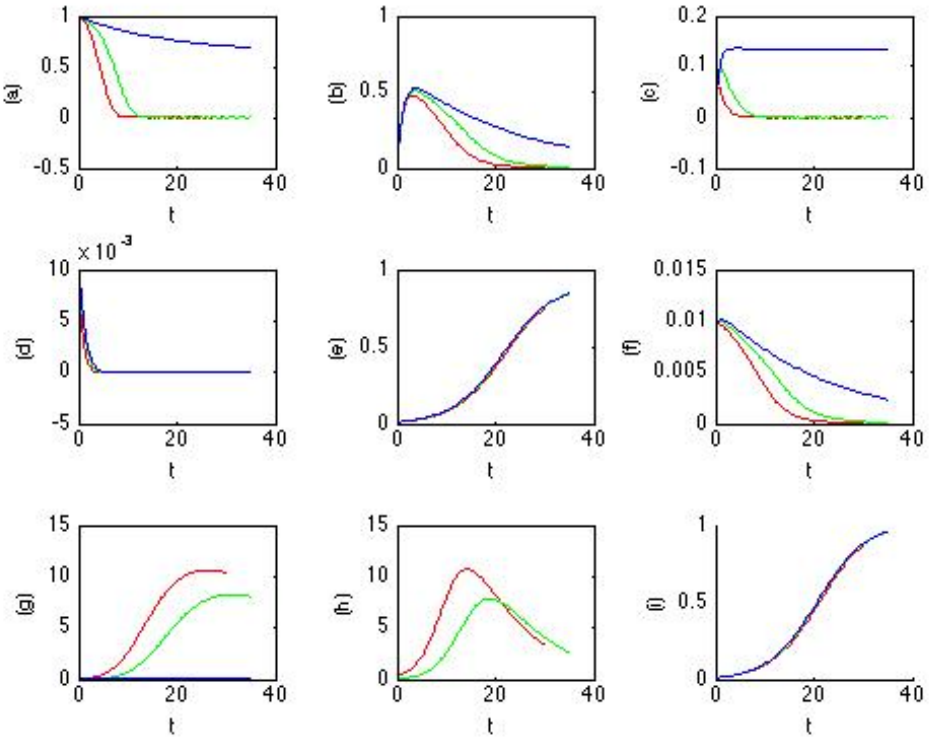

Figure 4-2 Simulation of Fibrocyte Model Temporal Dynamics:
(a) Mast cell, (b) Pro-Inflammatory Chemoattractants, (c) Regulatory Chemoattractants, (d) Fibrocyte, (e) Fibroblasts, (f) Inflammatory Macrophages, (g) Regulatory Macrophages (h) MSC (i) ECM population temporal dynamics with red representing the highest initial stem cell coating (5), green the second highest (.1) and blue no stem cell

As Fibrocyte cell populations continue to draw the attention of researchers in the fibrotic reaction field a greater understanding of parameter values and reactions can be incorporated. Once this is achieved, modeling considerations will likely reveal a greater influence by fibrocytes on healing processes. For now, the lack of impact on the temporal dynamics of our model justified our exclusion of the fibrocyte term at the current time, allowing us to focus in greater detail on the effects of Mesenchymal Stem cells on macrophage phenotype dynamics.

References

[1] Anderson, J.M., Rodriguez, A. and Chang, D.T. “Foreign body reaction to biomaterials.” *Semin Immunol* 20, 86-100. 2008.

[2] Kawahara, H., “Cellular responses to implant materials: biological, physical and chemical factors”. *Int Dent J* 33, 350-75. 1983

[3] Luttikhuizen, D.T., Harmsen, M.C. and Van Luyn, M.J., “Cellular and molecular dynamics in the foreign body reaction”. *Tissue Eng* 12, 1955-70. 2006

[4] Tang, L. and Eaton, J.W., “Inflammatory responses to biomaterials”. *Am J Clin Pathol* 103, 466-71. 1995

[5] Zhou, J., Tsai, Y.T., Weng, H., Baker, D.W. and Tang, L., “Real time monitoring of biomaterial-mediated inflammatory responses via macrophage-targeting NIR nanoprobes”. *Biomaterials* 32, 9383-90. 2011.

[6] Thevenot, P.T., Baker, D.W., Weng, H., Sun, M.W. and Tang, L. “The pivotal role of fibrocytes and mast cells in mediating fibrotic reactions to biomaterials.” *Biomaterials* 32, 8394-403. 2011

[7] Appling, W.D., O'Brien, W.R., Johnston, D.A. and Duvic, M. “Synergistic enhancement of type I and III collagen production in cultured fibroblasts by transforming growth factor-beta and ascorbate”. *FEBS* Lett 250, 541-4,1989.

[8] Fujiwara, N. and Kobayashi, K., “Macrophages in inflammation”. *Curr Drug Targets Inflamm Allergy* 4, 281-6. 2005.

[9] Streuli, C.H., Schmidhauser, C., Kobrin, M., Bissell, M.J. and Derynck, R., “Extracellular matrix regulates expression of the TGF-beta 1 gene”. *J Cell Biol* 120, 253-60. 1993.

[10] Zdolsek J, Eaton JW, Tang L. "Histamine Release and Fibronogen Absorption Mediate Acute Inflammatory Responses to Biomaterial implants in Humans". *Journal of Translational Medicine* 5:31. 2007

[11] Lemon G, Waters SL, Rose FR, King JR. "Mathematical modeling of human mesenchymal stem cell proliferation and differentiation inside artificial porous scaffolds". *J Theor Biol.* 249(3):543-53. 2007

[12] Wu, Chen, Scott and Tredget. "Mesenchymal Stem Cells Enhance Wound Healing Through Differentiation and Angiogenesis" *Stem Cells.* 25:2648-2559.2007

[13] D. M. Mosser and J. P. Edwards, "Exploring the full spectrum of macrophage activation," *Nature Reviews Immunology*, vol.8, no. 12, pp. 958–969, 2008.

[14] Khallou-Laschet, J., Varthaman, A., Fornasa, G., Compain, C., Gaston, A.T., Clement, M., Dussiot, M., Levillain, O., Graff-Dubois, S., Nicoletti, A., Caligiuri, G., 2010. "Macrophage plasticity in experimental atherosclerosis." *PLoS One 5*, e8852.

[15] Murray, P.J. and Wynn, T.A. "Protective and pathogenic functions of macrophage subsets." *Nat Rev Immunol* 11, 723-37. 2011.

[16] Fadok VA, Bratton DL, Konowal A, Freed PW, Westcott JY and Henson PM (1998) Macrophages that have ingested apoptotic cells in vitro inhibit proinflammatory cytokine production through autocrine/paracrine mechanisms involving TGFβ, PGE2, and PAF. J. Clin. Invest. 101: 890-898

[17] Clancy RM and Buyon JP, "Clearance of apoptotic cells: TGFβ in the balance between inflammation and fibrosis", *Journal of Leukocyte Biology*, 74:959-960. 2003

[18] Loke P, Gallagher J, Nair MG, Zang X, Brombacher F, Mohrs M, Allison JP and Allen JE. "Alternative activation is an innate response to injury that requires CD4+ T cells to be sustained during chronic infection", *J. Immunol.* 179: 3926-3936. 2007

[19] Gordon S and Taylor PR. "Monocyte and macrophage heterogeneity", *Nature Rev. Immunol.* 5: 953-964. 2005

[20] Reynolds, A., Rubin, J., Clermont, G., Day, J., Yodovotz, Y., Ermentrout, G. B., "A reduced mathematical model of the acute inflammatory response: I. Derivation of the model and analysis of anti- inflammation." *J. Theor. Biol.* 242, 220-236. doi:10.1016/j.jtbi.20006.02.016. 2006.

[21] Tang L. Jennings TA, Eaton JW. "Mast Cells Mediate acute inflammatory responses to implanted biomaterials". *Proc. Natl. Acad. Sci.* Vol. 95 pp. 8841-8846. 1998

[22] McDonald JA "Fibronectin: a primitive matrix. In The molecular and cellular biology of wound repair" *New York: Plenum Press.* (ed. R. A. F. Clark, P.M. Henson), pp. 405-436. 1988

[23] Goldberg B, "Kinetics of processing of type I and type III procollagens in fibroblast cultures", *Proc Natl Acad Sci* U S A., 74(8): 3322-3325. 1977.

[24] Stricklin, G.P., Eisen, A.Z., Bauer, E.A. and Jeffrey, J.J., "Human skin fibroblast collagenase: chemical properties of precursor and active forms". *Biochemistry* 17, 2331-7. 1978

[25] R. Schugart, A. Friedman, R. Zhao, and C.K. Sen. "Wound angiogenesis as a function of tissue oxygen tension – a mathematical model". *PNAS*, 105, pp 2628-33, 2008.

[26] Pettet, G.J., Byrne, H.M., McElwain, D.L. and Norbury, J. "A model of wound-healing angiogenesis in soft tissue", *Math Biosci* 136, 35-63.1996.

[27] J. Flegg, J.A.Thackham, D.L.S. McElwain, R.J.Long. "Hyperbaric Oxygen Therapy to Treat Chronic Wounds:A Review" *Wound Repair and Regeneration.* 16:321-330. 2008

[28] Thevenot P, Ashwin N, Parisa L, Cheng-Yo K, Tang L. "The effect of incorporation of SDF-1α into PLGA scaffolds on stem cell recruitment and the inflammatory response". *Biomaterials* 31 3997-4008. 2010

[29] Greg Lemon, Daniel Howard, Matthew J. Tomlinson, Lee D. Buttery, Felicity R.A.J. Rose, Sarah L. Waters, John R. King. "Mathematical modeling of tissue-engineered angiogenesis". *Mathematical Biosciences* 221:101–120. 2009

[30] Han S, Chun K, Gye M, Kim W. "The Effect of Human Bone Marrow Stromal Cells and Dermal Fibroblasts on Angiogenesis". *Plast. Reconstr. Surg.* 117:829. 2006.

[31] Sudeepta Aggarwal, Mark F. Pittenger. "Human Mesenchymal Stem Cells Modulate Allogeneic Immune Cell Responses". *Blood Journal* 105:1815-1822. 2005

[32] P. D. Dale, J. A. Sherratt, and P. K. Maini, "A mathematical model for collagen fibre formation during foetal and adult dermal wound healing," *Proceedings of the Royal Society B*, vol. 263, no. 1370, pp. 653–660, 1996.

[33] Dale PD, Sherratt JA and Maini PK. "The role of fibroblast migration in collagen fibre formation during foetal and adult dermal wound healing," *Bull. Math. Biol.* 59(6):1077-1100. 1997

[34] Dallon JC, Sherratt JA and Maini PK. "Modeling the effects of transforming growth factor-β on extracellular matrix alignment in dermal wound repair," *Wound Repair and Regeneration*, 9:278-286. 2001

[35] Helen V. Waugh, Jonathan A. Sherrat. "Macrophage Dynamics in Diabetic Wound Healing". *Bulletin of Mathematical Biology.* 68:197-207, 2006.

[36] Keener, James; Sneyd, James. Mathematical Physiology I: Cellular Physiology. Interdisciplinary Applied Mathematics 8/1 (2 ed.). New York: Springer, 1998.

[37] Day, J., Rubin, J., Vodovotz, Y., Chow, C.C., Reynolds, A., Clermont, G., "A reduced mathematical model of the acute inflammatory response: II. Capturing scenarios of repeated endotoxin administration." *J. Theor. Biol.* 242, 37-256. doi:10.1016/j.jtbi.20006.02.015. 2006

[38] Ibragimov A., Ritter L. R. and Walton J. R., "Stability Analysis of a Reaction-Diffusion System Modeling Atherogenesis," *SIAM J. Appl. Math.*, 70(7), pp. 2150-2185. 2010

[39] J. Su, M Todorov, H. Perez, L. Perkins, H Kojouharov, H. Weng, L. Tang, "A predictive tool for foreign body fibrotic reactions using a two-dimensional computational model", *Open Access Bioinformatics*, 2011:3, pp 19-35, 2011.

[40] Jain HV, Moldovan NI, Byrne H. "Modeling Stem/Progenitor Cell-Induced Neovascularization and Oxygenation Around Solid Implants". *Tissue Eng Part C Methods*. 2012 Jul;18(7):487-95. 2012.

[41] Yang J, Su J, Owens L, Ibraguimov A, Tang L. "A computational model of fibroblast and macrophage spatial/temporal dynamics in foreign body reactions," *Journal of Immunological Methods,* Vol. 397, Issue 1-2, pages 37-46, 2013.

[42] A. Ibraguimov, L. Owens, J. Su, and L. Tang, "Stability Analysis of a Model for Foreign Body Fibrotic Reactions," *Computational and Mathematical Methods in Medicine*, vol. 2012, Article ID 809864.doi:10.1155/2012/809864, 2012.

[43] Dey, J., Tran, R.T., Shen, J., Tang, L. and Yang, J. "Development and long-term in vivo evaluation of a biodegradable urethane-doped polyester elastomer." *Macromolecular materials and engineering* 296, 1149-1157. 2011.

[44] Baker, D.W., Liu, X., Weng, H., Luo, C. and Tang, L. "Fibroblast/fibrocyte: surface interaction dictates tissue reactions to micropillar implants." *Biomacromolecules* 12, 997-1005. 2011.

[45] Enholm, B., Paavonen, K., Ristimaki, A., Kumar, V., Gunji, Y., Klefstrom, J., Kivinen, L., Laiho, M., Olofsson, B., Joukov, V., Eriksson, U. and Alitalo, K. "Comparison of VEGF, VEGF-B, VEGF-C and Ang-1 mRNA regulation by serum, growth factors, oncoproteins and hypoxia*" Oncogene* 14, 2475-83. 1997.

[46] Ristimaki, A., Narko, K., Enholm, B., Joukov, V. and Alitalo, K."Proinflammatory cytokines regulate expression of the lymphatic endothelial mitogen vascular endothelial growth factor-C", *J Biol Chem* 273, 8413-8. 1998

[47] Olsen, L., Sherratt, J.A. and Maini, P.K. "A mechanochemical model for adult dermal wound contraction and the permanence of the contracted tissue displacement profile." *J Theor Biol* 177, 113-28. 1995.

[48] Hackam, D.J. and Ford, H.R. "Cellular, biochemical, and clinical aspects of wound healing". *Surg Infect* (Larchmt) 3 Suppl 1, S23-35. 2002.

[49] Blankson, J., Persaud, D. and Siliciano, R.F. "Latent reservoirs for HIV-1". *Curr Opin Infect* Dis 12, 5-11. 1999

[50] Namy, P., Ohayon, J. and Tracqui, P. "Critical conditions for pattern formation and in vitro tubulogenesis driven by cellular traction fields*". J Theor Biol* 227, 103-20. 2004.

[51] Ellis I., Grey A.M., Schor A.M. and Schor S. L., "Antagonistic effects of TGFβ-1 and MSF on fibroblast migration and hyaluronic acid synthesis Possible implications for dermal wound healing, *Journal of Cell Science*, 102, pp. 447-456.1992.

[52] Ibragimov, A. I., McNeal, C. J., Ritter, L. R., Walton, J. R. "Stability analysis of a model of atherogenesis: an energy estimate approach." *Comput. Math. Methods Med. 9* (2008)

[53] Xue C. , Friedman A., and Sen C. K. "A mathematical model of ischemic cutaneous wounds," *Proceedings of the National Academy of Sciences*, 106, pp16782-16787. 2009

[54] Arciero J.C., Mi Q. , Branca M.F , Hackam D. , and Swigon D. , "Two-dimensional continuum mechanical model of collective cell migration", *Biophys. J.*, 100, 535-543. 2011

[55] Nowak M.A. Bangham C.R.M, "Population Dynamics of Immune Responses to Persistent Viruses", *Science*, New Series, Volume 272, Issue 5258, pp. 74-79.1996.

[56] J.D.Murray. “Parameter space for turing instability in reaction diffusion mechanisms: A comparison of models”. *Journal of Theoretical Biology,* Volume 98, Issue 1, p.143-163.1982.

[57] Paul Thevenot, Wenjing Hu, and Liping Tang. “Surface Chemistry Influence Implant Biocompatibility*”. Curr Top Med Chem*. 8(4): 270–280. 2008

[58] Seung-Kyu Han, Tae-Hwan Yoon, Dong-Geun Lee, Min-Ah Lee, Woo-Kyung Kim. “Potential of human bone marrow stromal cells to accelerate wound healing in vitro”. *Ann Plast Surg* 55(4):414-9. 2005

[59] Jeong-Bae Kim, Kyung-Wook Chun, Seung-Kyu Han, Woo-Kyung Kim. “Effect of human bone marrow stromal cell allograft on proliferation and collagen synthesis of diabetic fibroblast in vitro”. *Journal of Plastic, Reconstructive and Aesthetic* Surgery (2010) 63, 1030-1035. 2010

[60] Reikoff R., Bucala R., Herzog E. “Fibrocytes: emerging effector cells in chronic inflamation”. *Nature Reviews Immunology.*11:427-435, 2011.

[61] Omar I. Butt, Robert Carruth, Vijay K. Kutala, Periannan Kuppusamy, and Nicanor I. Moldovan. “Stimulation of Peri-Implant Vascularization with Bone Marrow-Derived Progenitor Cells: Monitoring by In Vivo EPR Oximetry”. *Tissue Engineering*. 13(8): 2053-2061. 2007

[62] Mori, L., Bellini A.,Stacey M, Schmidt M, Mattoli S. “Fibrocytes contribute to the myofribroblast population in wounded skin and originate from the bone marrow”. Experimental Cell Research 304 (2005) 81-90.

Biographical Information

Larrissa Owens, maiden name Perkins, born May 4th, 1987 in Santa Clarita California, graduated Summa Cum Laude with a Bachelor of Science in Mathematics and Secondary Education from Howard Payne University in 2009. While at HPU she received the Top Graduate Award, the Outstanding Senior in Mathematics Education, and the Pre-Teacher Service Award and completed teacher certification for Mathematics 8-12. She accepted the US Department of Education GAANN Fellowship at the University of Texas at Arlington the next fall and in December 2011 received a Master of Science Degree in Mathematics for her work under advisor Jianzhong Su, Ph.D. She continued her graduate studies under Dr. Su and received further funding and teaching experience as a National Science Foundation GK12 MAVS Fellow.

During her time at UTA she contributed to the publication of four research articles: "A computational model of fibroblast and macrophage spatial/temporal dynamics in foreign body reactions," *Journal of Immunological Methods* (2013), "Stability Analysis of a Model for Foreign Body Fibrotic Reactions," *Computational and Mathematical Methods in Medicine* (2012), "A Predictive Tool for Foreign Body Fibrotic Reactions using a Two-Dimensional Computational Model", *Open Access Bioinformatics* (2011), and "Predicting Foreign Body Reactions Using Computational Model-The Multiple Roles of Macrophages". *International Journal of Medical Implant and Devices*. (2011). She received the Peer Mentor Award, the Outstanding GAANN Fellow Award, the ACES NSF GK-12 Best Presentation Award, and the Outstanding Performance in Integrating Applied Math Research in the K-12 Classroom.

After she graduates with a Doctorate in Mathematics from UTA in May 2014, Larrissa plans to continue in her passions of teaching students how to explore mathematics. Larrissa enjoys shaping young mathematical minds and aims to continue mentoring and sparking student curiosity about mathematics in a classroom of her own.